Molecular Therapy
Original Article

Reactive oxygen species-responsive nanocarrier ameliorates murine colitis by intervening colonic innate and adaptive immune responses

Xiangji Yan,[1,2,9] Lingzhang Meng,[3,4,9] Xingzhe Zhang,[5,6] Zhichao Deng,[1,2] Bowen Gao,[1,2] Yujie Zhang,[1,2] Mei Yang,[1,2] Yana Ma,[1,2] Yuanyuan Zhang,[1,2] Kangsheng Tu,[1] Mingzhen Zhang,[1,2] and Qiuran Xu[7,8]

[1]Department of Hepatobiliary Surgery, the First Affiliated Hospital, School of Basic Medical Sciences, Xi'an Jiaotong University, Xi'an, Shaanxi 710061, China; [2]Key Laboratory of Environment and Genes Related to Diseases, Xi'an Jiaotong University, Ministry of Education, Xi'an, Shaanxi 710061, China; [3]Institute of Cardiovascular Sciences, Guangxi Academy of Medical Sciences, Nanning, Guangxi 530021, China; [4]Center for Systemic Inflammation Research (CSIR), Youjiang Medical University for Nationalities, Baise, Guangxi 533000, China; [5]Department of Pathogenic Microbiology and Immunology, School of Basic Medical Sciences, Xi'an Jiaotong University, Xi'an, Shaanxi 710061, China; [6]Xi'an Key Laboratory of Immune Related Diseases, Xi'an, Shannxi 710061, China; [7]Laboratory of Tumor Molecular Diagnosis and Individualized Medicine of Zhejiang Province, Zhejiang Provincial People's Hospital, Affiliated People's Hospital, Hangzhou Medical College, Hangzhou, Zhejiang 310014, China; [8]Research Center of Diagnosis and Treatment Technology for Hepatocellular Carcinoma of Zhejiang Province, Hangzhou, Zhejiang 310009, China

Ulcerative colitis (UC) is a chronic or relapsing inflammatory disease with limited therapeutic outcomes. Pterostilbene (PSB) is a polyphenol-based anti-oxidant that has received extensive interest for its intrinsic anti-inflammatory and anti-oxidative activities. This work aims to develop a reactive oxygen species (ROS)-responsive, folic acid (FA)-functionalized nanoparticle (NP) for efficient PSB delivery to treat UC. The resulting PSB@NP-FA had a nano-scaled diameter of 231 nm and a spherical shape. With ROS-responsive release and ROS-scavenging properties, PSB@NP could effectively scavenge H_2O_2, thereby protecting cells from H_2O_2-induced oxidative damage. After FA modification, the resulting PSB@NP-FA could be internalized by RAW 264.7 and Colon-26 cells efficiently and preferentially localized to the inflamed colon. In dextran sulfate sodium (DSS)-induced colitis models, PSB@NP-FA showed a prominent ROS-scavenging capacity and anti-inflammatory activity, therefore relieving murine colitis effectively. Mechanism results suggested that PSB@NP-FA ameliorated colitis by regulating dendritic cells (DCs), promoting macrophage polarization, and regulating T cell infiltration. Both innate and adaptive immunity were involved. More importantly, the combination of the PSB and dexamethasone (DEX) enhanced the therapeutic efficacy of colitis. This ROS-responsive and ROS-scavenging nanocarrier represents an alternative therapeutic approach to UC. It can also be used as an enhancer for classic anti-inflammatory drugs.

INTRODUCTION

Ulcerative colitis (UC) is an inflammatory disease that occurs in the colon caused by an interaction of genetics, immune responses, and environmental factors, and is characterized by alternating periods of disease onset and remission.[1,2] It begins at the rectum and extends to the entire colon, resulting in significant disturbance of colon homeostasis and severe damage to intestinal barrier function.[3] Common symptoms of active UC include abdominal pain, diarrhea, weight loss, and rectal bleeding.[4] UC is prone to colon cancer if not effectively treated, leading to life-threatening consequences.[3,5]

There are many factors involved in the occurrence and development of UC. Among them, reactive oxygen species (ROS) are closely associated with the pathological process of UC.[6] Although ROS at low levels can effectively regulate cellular signaling and oxygen homeostasis, high levels of ROS can cause cell damage during oxidative stress.[7] A large number of immune cells infiltrate the inflamed colon tissues in the pathological process of UC, producing a large amount of ROS, inducing cell oxidative stress damage, and exacerbating the inflammatory response.[8] H_2O_2 is the most abundant and stable non-radical ROS in cells.[8] In addition, T lymphocytes and their cytokines also play an important role in regulating gut immune responses and in the pathogenesis of intestinal inflammation.[9] In healthy intestinal mucosa, T lymphocytes maintain intestinal homeostasis and maintain autoimmune tolerance and resistant stability.[10] Intestinal immune

Received 25 August 2022; accepted 22 February 2023;
https://doi.org/10.1016/j.ymthe.2023.02.017.

[9]These authors contributed equally

Correspondence: Kangsheng Tu, Department of Hepatobiliary Surgery, the First Affiliated Hospital, School of Basic Medical Sciences, Xi'an Jiaotong University, Xi'an, Shaanxi 710061, China.
E-mail: tks0912@foxmail.com
Correspondence: Mingzhen Zhang, Department of Hepatobiliary Surgery, the First Affiliated Hospital, School of Basic Medical Sciences, Xi'an Jiaotong University, Xi'an, Shaanxi 710061, China.
E-mail: mzhang21@xjtu.edu.cn
Correspondence: Qiuran Xu Laboratory of Tumor Molecular Diagnosis and Individualized Medicine of Zhejiang Province, Zhejiang Provincial People's Hospital, Affiliated People's Hospital, Hangzhou Medical College, Hangzhou, Zhejiang 310014, China.
E-mail: windway626@sina.com

responses of patients with UC are often characterized by activation and infiltration of lamina propria T lymphocytes (LPLs) with potent effector functions, releasing cytokine, histamine, and proteases.[11,12] $CD4^+$ T lymphocytes account for 60% to 70% of T cells in the LPL and have a significant contribution to the pathogenesis of UC.[13] Thus, the altered bowel physiology of patients with UC may relate to immune mechanisms.

Clinically, for treatment, UC is generally managed by traditional methods, including 5-aminosalicylic acid, corticosteroids, immunosuppressive agents, and monoclonal antibodies.[14] Most of these treatments are anti-inflammatory drugs, which have potentially serious side effects and only control the condition within a short time.[2] There are still a large number of patients who cannot be relieved by drugs and require surgery.[15] However, due to the complex etiology and various symptoms of UC, the treatment effect is still not ideal. Therefore, it is necessary to develop safe and effective drugs for the treatment of UC.

Pterostilbene (PSB), a natural phenolic compound, is widely distributed in various natural medicinal plants.[16,17] PSB has attracted considerable attention due to its good biocompatibility and bioactivity. It has anti-oxidant, anti-inflammatory,[18,19] anti-cancer,[20] and anti-cardiovascular properties, and so can improve the function of normal cells, inhibit malignant cells, and effectively treat and prevent human diseases.[21] It has been shown to have preventive and therapeutic effects on a variety of human diseases, including colitis, neurological, cardiovascular, and hematologic diseases, and can effectively scavenge free radicals.[22] Recently, the anti-inflammatory effect of PSB has been used as alternative therapy for patients with UC who failed to be treated with traditional drugs.[23] However, the poor oral effect, low targeting efficiency, rapid plasma clearance, and poor water solubility limit the use of PSB for further application.[24] The ideal state of the drug delivery system in UC treatment is to deliver the drug to the inflamed colon at a maximum dose to minimize systemic drug exposure. Therefore, there is an urgent need to develop a drug delivery system to solve the above-mentioned problems, such as targeting delivery capabilities and high drug encapsulation efficiency.

As a US Food and Drug Administration (FDA)-approved polymer, poly(lactic-co-glycolic acid) (PLGA) is permitted to be used in clinical treatment. It can effectively solve the above problems, including improving the bioavailability of drugs, colon targeting, and controlled release.[25,26] The PLGA polymer-based nano-drug delivery system has the characteristics of a simple synthesis method, high stability, improved drug solubility, and slow release of encapsulated drugs.[27,28] Polyethylene glycol (PEG) has good amphiphilic and biosafety and has been approved by FDA because of its low toxicity. PEG modification can improve the long circulation time of nanoparticles (NPs) *in vivo*, thus avoiding being cleared by the reticuloendothelial system (RES), reducing immunogenicity, and improving the biocompatibility of NPs. In addition, passive targeting is achieved through the enhanced permeability and retention (EPR) effect due to increased tissue permeability at the site of inflammation.[29,30] By modifying the targeting molecule, the NPs can be actively targeted to the inflammatory tissue, reducing systemic exposure, increasing the accumulation of drugs in the inflammatory site, and enhancing the drug's efficacy. More and more studies show that PLGA-based nano-drug delivery systems can effectively treat UC,[31–34] which may be an alternative approach in the nanotherapeutics of UC.

In this work, an ROS-responsive (thioketal linkage), folic acid (FA)-functionalized nanocarrier for efficient PSB delivery (PSB@NP-FA) to the inflamed colon was designed. With ROS-responsive and ROS-scavenging properties, PSB@NP could effectively scavenge H_2O_2, thereby protecting RAW 264.7 cells from H_2O_2-induced oxidative damage. Mediated by FA targeting, PSB@NP-FA could be internalized by RAW 264.7 cells and Colon-26 cells efficiently *in vitro* and preferentially localized to the inflamed colon after intravenous administration. PSB@NP-FA ameliorated UC efficiently by regulating DCs and colonic M1/M2 macrophage polarization (two kinds of cells mainly involved in innate immune responses) and T cell infiltration (Figure 1). More importantly, the combination of the PSB and dexamethasone (DEX) enhanced the therapeutic efficacy of colitis. Without appreciable systemic toxicity, this nanocarrier represents an alternative therapeutic approach to UC, and it can also be used as a synergist for classic anti-inflammatory drugs of UC.

RESULTS

Characterization of PSB@NP-FA

NPs require precise size and morphology modulation to adapt to the pathological conditions of different diseases.[35] Based on the characteristics of PEG-modified PLGA, we used them to encapsulate drugs by adjusting and optimizing the ratio of the PLGA-PEG derivatives and drugs to synthesize optimized PSB@NPs and DEX/PSB@NPs with superior performance and high encapsulation efficiency. As shown in Figure 2A, transmission electron microscopy (TEM) images showed that the morphology of PSB@NP-FA had a regularly spherical shape and smooth surface, indicating the successful preparation of PSB@NP-FA. As measured by dynamic light scattering (DLS), the average diameter of the NPs was 231.6 nm with low polydispersity index (PDI) less than 0.1 (Figure 2B). The zeta potential of PSB@NP-FA was about -21.8 ± 1.76 mV (Figure 2C). A UV-visible (UV-vis) spectrophotometer was used to measure the loading capacity (LC%) and encapsulation efficiency (EE%) of PSB in NPs by establishing a standard curve (Figures S1A and S1B). By adjusting the ratio of polymer/PSB, the optimal encapsulation rate was obtained when PSB was at 2.5 mg (Figure S1C). Under this condition, the EE% and LC% of PSB@NP-FA are 85.27% ± 0.51% and 3.74% ± 2.69%, respectively (Figure S1C).

Fourier transform infrared spectroscopy (FTIR) was used to characterize the successful synthesis of PSB@NP (Figure 2D). In the FTIR spectrum of Mal (maleimide), TK (thioketal), and NP (PSB@NP), the benzene skeleton of Mal and the carboxyl bond of TK produced characteristic peaks with obvious tensile vibration at 1,487.51 cm^{-1}, 1,895.24 cm^{-1}, and 1,210.98 cm^{-1}. The FTIR spectra of characteristic peaks verified the successful conjugation of TK linkage, which could

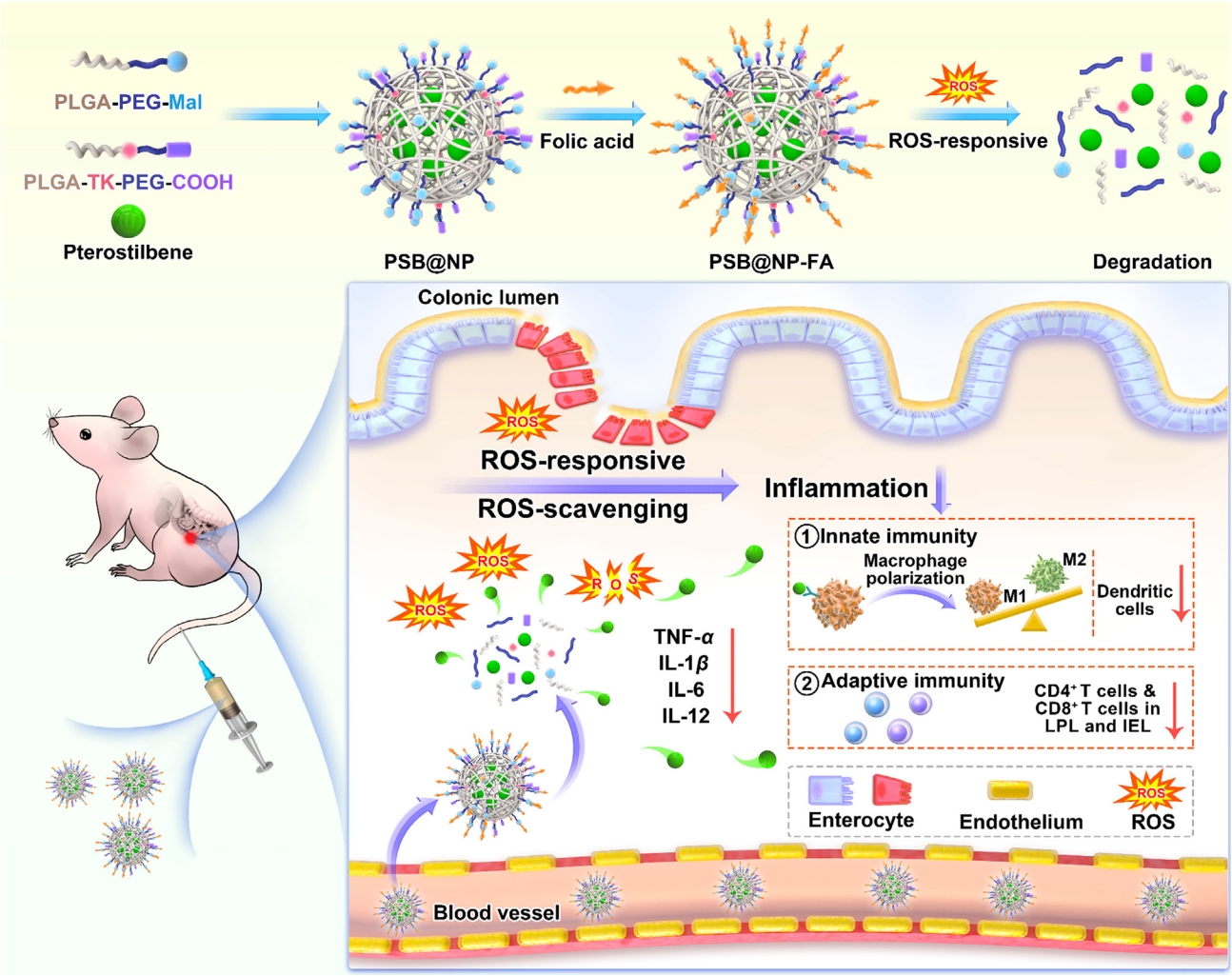

Figure 1. Schematic diagram of the ROS-responsive nanocarrier ameliorates murine colitis

PSB@NP-FA were synthesized by a single microemulsion method and could be cleaved under ROS stimulation. Upon intravenous injection, PSB@NP-FA preferentially localized to the inflamed colon and ameliorated murine colitis via regulating colonic DCs, M1/M2 macrophage polarization, and T cell infiltration.

be rapidly cleaved in response to ROS stimulation. FA can bind to FA receptors with high affinity, and FA receptors were highly expressed in the inflamed colonic mucosa.[36,37] Hence, we used FA to functionalize PSB@NP to endow the colon inflammation-targeting ability. The FTIR spectrum showed that the absorption peak of FA appeared at 2,953.75 cm^{-1}, 1,251.71 cm^{-1}, and 912.59 cm^{-1} (Figure S2). After FA conjugation, the amide stretch vibrations at 1,554.57 cm^{-1} appeared, indicating the successful conjugation of FA with PSB@NP-FA.

PSB@NP is designed to degrade in an ROS-triggered manner. When PSB@NP is placed in the ROS environment, the thioketal linker in PLGA-TK-PEG-COOH will be cleaved to form ketones and mercaptan. The morphology of PSB@NP will be destroyed, and gradually cracked, and the PSB will be released from PSB@NP. H_2O_2, a member of ROS, was used to measure the drug-release ability of PSB@NP under the stimulation of ROS. We compared the drug-release rates of TK-based NPs (PSB@PLGA-TK-PEG) and PLGA-based NPs (PSB@PLGA) in solution with or without H_2O_2 (10 μM) at different pH values (6.5 or 7.4). As presented in Figure 2E, the cumulative release of PSB@PLGA-TK-PEG reached 85.1% within 48 h in a solution containing H_2O_2 at pH 6.5, while the cumulative release of PSB@PLGA was only 66.8%. The cumulative release of PSB@PLGA-TK-PEG without H_2O_2 was 20% less than with H_2O_2 over 48 h. A similar result was also observed at pH 7.4 (Figure 2F), and the release amounts of PSB@PLGA and PSB@PLGA-TK-PEG in the presence of H_2O_2 were 59.3% and 86.2%, respectively. In the absence of H_2O_2, the release of the PSB@PLGA was around 56.4%, which was similar to PSB@PLGA-TK-PEG. These results showed that PSB@PLGA-TK-PEG had ROS-responsive drug-release ability,

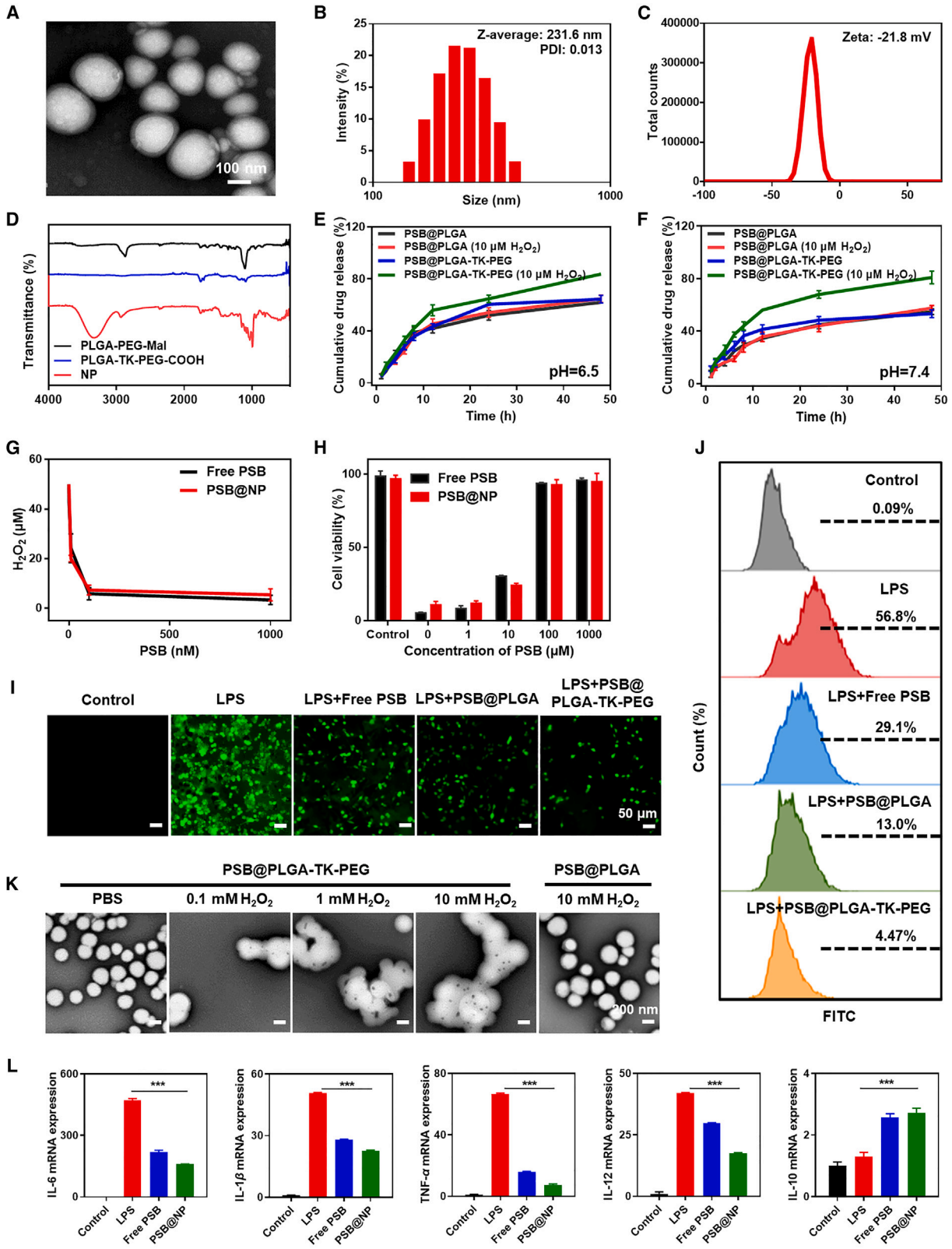

(legend on next page)

which might be due to the destruction of the structure of NP caused by TK bond fracture, leading to the release of encapsulated drugs. Moreover, higher release efficiency of PSB@PLGA-TK-PEG was observed at pH 6.5 compared with pH 7.4 (Figures 2E and 2F), suggesting that the ROS-responsive drug release may be further improved in an acidic environment.

ROS-scavenging and ROS-responsive properties of PSB@NP *in vitro*

With the occurrence and development of UC, the concentration of ROS in intestinal cells increased in the course of inflammatory and immune activation, which further exacerbated the disease.[8,38] We next examined whether PSB@NP retained the ROS-scavenging capability based on PSB presence. H_2O_2 is one of the most abundant and stable ROS in the body. As shown in Figure 2G, when the PSB@NP or the free PSB was mixed with H_2O_2, the remaining H_2O_2 decreased significantly along with the increased concentration of PSB. Excitingly, 1 μM free PSB and PSB@NP (equal to PSB) could scavenge 50 μM H_2O_2. There was no significance between free PSB and PSB@NP, indicating PSB in NPs still retained its original anti-oxidant capability. Next, the protective effect of free PSB and PSB@NP on cells from ROS-induced oxidative damage was investigated. When treated with H_2O_2 to cause oxidative stress, the cell viability was significantly decreased. When pre-treated with free PSB and PSB@NP, the cell viability was rescued considerably in a concentration-dependent manner (Figure 2H). These findings suggested that PSB@NP retained the anti-oxidant capability of PSB and could protect RAW 264.7 cells from ROS-induced oxidative stress.

DCFH-DA (2,7-dichlorodihydrofluorescein diacetate), a general ROS probe, was also used to assess the anti-oxidant capability of PSB@NP. As shown in Figure 2I, in the negative control group, RAW 264.7 cells showed a tiny DCFH-DA fluorescence signal, indicating a few productions of ROS. In contrast, in the positive control group (LPS (Lipopolysaccharide) group), a large amount of DCFH-DA fluorescence signal was detected, indicating that LPS treatment significantly increased ROS level in RAW 264.7 macrophages (Figure 2I). After being pre-treated with free PSB, PSB@PLGA, or PSB@PLGA-TK-PEG, when compared with the positive control group, the DCFH-DA fluorescence signal decreased significantly (Figure 2I), indicating that free PSB, PSB@PLGA, and PSB@PLGA-TK-PEG had the scavenging capability of ROS, and ROS-scavenging ability was mainly played by PSB instead of thioketal moiety. Flow cytometry results were consistent with fluorescence imaging (Figure 2J). These results indicated that LPS could induce the production of intracellular ROS, and PSB treatment could effectively remove ROS and protect cells from oxidative stress damage.

To further investigate the ROS-responsive properties of PSB@NP, the morphology of PSB@NP under H_2O_2 conditions were observed by TEM. The TEM images showed that the morphology of PSB@PLGA-TK-PEG remained intact in PBS (Figure 2K). When added to H_2O_2, PSB@PLGA-TK-PEG degraded gradually, and the complete structure of PSB@PLGA-TK-PEG disappeared in all tested H_2O_2 concentrations (Figure 2K), which should be attributed to the thioketal linkages in the polymer being quickly oxidized and cleaved by H_2O_2. However, the morphology of PSB@PLGA without ROS-responsive properties remained intact even in 10 mM H_2O_2 solution (Figure 2K). These findings suggested the ROS-responsive performance of PSB@PLGA-TK-PEG, indicating the potential to be a controlled delivery carrier.

Anti-inflammatory effect of PSB@NP *in vitro*

Inflammatory factors are involved in the occurrence and development of UC, and the imbalance of inflammatory factors and the severe increase of pro-inflammatory factors further aggravate the inflammatory response.[39] Next, we studied the anti-inflammatory effects of PSB at the cellular level. Interleukin (IL)-6, IL-1β, tumor necrosis factor alpha (TNF-α), and IL-12 are the major pro-inflammatory cytokines secreted by M1 macrophages during inflammation. We used LPS to stimulate RAW 264.7 macrophages to secrete pro-inflammatory cytokines and then observed whether pretreatment with free PSB or PSB@NP could reduce their expression. Results showed that the expression of IL-6, IL-1β, TNF-α, and IL-12 were upregulated in the LPS-treated group compared with the untreated control group (Figure 2L). Strikingly, the mRNA level of pro-inflammatory cytokines in the free PSB and PSB@NP pre-treated group decreased significantly (Figure 2L). Meanwhile, the expression of IL-10, a main anti-inflammatory cytokine secreted by M2 macrophages, increased after PSB treatment (Figure 2L), indicating that PSB could effectively eliminate LPS-induced inflammation and have an anti-inflammatory effect, and PSB@NP could have better anti-inflammatory effects than free PSB.

Cellular uptake of PSB@NP-FA by macrophages and colon-26 cells

Efficient anti-inflammatory drug delivery can increase drug concentration in the colon and improve cellular uptake of drugs, which is important for UC treatment.[40] In addition, efficient delivery can cut

Figure 2. Characterization and *in vitro* drug release, ROS-scavenging, ROS-responsive, and anti-inflammatory profiles of NPs

(A) Representative TEM images of PSB@NP-FA. Scale bar, 100 nm. (B) Representative size distribution and PDI of PSB@NP-FA (n = 3). (C) Zeta potential of PSB@NP-FA (n = 3). (D) FTIR analysis of the polymer materials and the PSB@NP-FA (NP). (E) The release profile of PSB from PLGA and PLGA-TK-PEG with or without H_2O_2 in solution (pH 6.5) (n = 3). (F) The release profile of PSB from PLGA and PLGA-TK-PEG with or without H_2O_2 in solution (pH 7.4) (n = 3). (G) The ROS-scavenging capacity of free PSB and PSB@NP was evaluated *in vitro*. (H) Cytoprotective effect of free PSB and PSB@NP was assessed by MTT assay. (I) DCFH-DA, a general ROS probe, was used to evaluate the anti-oxidant capability of free PSB, PSB@PLGA, and PSB@PLGA-TK-PEG. Scale bar, 50 μm. (J) Green fluorescence caused by ROS probe, DCFH-DA, was quantified by flow cytometry. (K) Representative TEM images of PSB@PLGA and PSB@PLGA-TK-PEG in H_2O_2 solution with different concentrations were obtained. Scale bar, 200 nm. (L) Inflammatory factors (IL-6, IL-1β, TNF-α, IL-12, and IL-10) were evaluated (n = 3).

down the dosage of administration and reduce the side effects of the drug. Folate receptor (FR) families include FR-α, FR-β, FR-γ, and FR-δ. FR-β is little or not expressed in most normal cells and highly expressed in cancer cells and activated RAW 264.7 cells.[36] Colon-26, a colon cancer cell, can be used as a colon epithelial-like cell to test cellular uptake of PSB@NP-FA. FA on the surface of PSB@NP-FA acts as a targeted molecule that binds specifically to FR-β. The results showed that the level of FR-β mRNA expression was low on NIH/3T3 cells and normal RAW 264.7 cells but was high on LPS-activated RAW 264.7 cells and Colon-26 cells (Figure 3A), confirming the feasibility of FA as a target molecule. We then qualitatively investigated the cellular uptake profiles of NPs using confocal microscopy to colon epithelial cells and RAW 264.7 macrophages. Confocal images showed that the PSB@NP-FA-labeled with DiL (1,1'-dioctadecyl-3,3,3',3'-tetramethylindocarbocyanine perchlorate) could be taken up by Colon-26 cells and RAW 264.7 cells, presenting a remarkable intracellular red fluorescence signal, which was stronger at 4 h (Figure 3C). The uptake capacity of cells pre-treated with FA was significantly reduced (FA + PSB@NP-FA group) (Figure 3C). Furthermore, the fluorescence intensity of DiL was also quantified by flow cytometry, which was consistent with the results of confocal images, indicating PSB@NP-FA could indeed target Colon-26 cells and RAW 264.7 cells (Figures 3D and 3E).

PSB@NP-FA preferentially localized to the inflamed colon

FR-β is expressed at sites of severe injuries, such as DSS-induced colitis in mice.[37] We detected the mRNA expression of FR-β in the colon of mice with colitis. The results showed that FR-β was not expressed in the colon of normal mice but was highly expressed in the colon tissues of mice with colitis (Figure 3B). To evaluate the colon-targeting ability of PSB@NP-FA, PSB@NP-FA-labeled by DiR (1,1'-dioctadecyl-3,3,3',3'-tetramethylindotricarbocyanine iodide) were intravenously administered to healthy mice and colitis mice. Images for the whole-body fluorescence distribution were acquired at 1, 2, 3, 6, 12, and 24 h after injection. Fluorescent images showed the highest fluorescence signal *in vivo* was detected at 3 h (Figures 3F and 3G). After sacrificing the mice, the main organs and colons of mice were imaged to observe the localization of NPs. Fluorescence images of major organs showed that the PSB@NP-FA were mainly distributed in the liver, spleen, and lung, and the fluorescence signal disappeared 24 h later, indicating that the PSB@NP-FA were gradually expelled from the body (Figures 3F and 3H). In addition, the fluorescence signal of colon tissues reached the highest at 3 h, indicating effective uptake of PSB@NP-FA in colon tissues (Figures 3F and 3I). Compared with the healthy mice, the fluorescence intensity in colitis mice was much stronger, indicating the effective targeting of PSB@NP-FA to the inflammation site (Figures 3F and 3I). The pharmacokinetic results showed that the fluorescence intensity of PSB@NP-FA decreased over time, and the half-life ($t_{1/2}$) of PSB@NP-FA in blood was 0.6169 ± 0.27 h (Figure 3J). We then observed the location of DiL-labeled NP in colonic frozen sections. Fluorescence images showed that the NPs were successfully targeted to the colon and taken up by colon epithelial cells (Figure S3). In conclusion, PSB@NP-FA are highly enriched in the inflammatory site of the colon but also gradually metabolized out of the body within 24 h, showing the good inflammation-targeting ability and biosafety of PSB@NP-FA.

Biocompatibility of NP

Biocompatibility is a prerequisite for the application of drug delivery platforms. We incubated different concentrations of Blank@NP and PSB@NP-FA with RAW 264.7 cells for different hours and detected cell viability by MTT (3-(4,5-dimethyl-2-thiazolyl)-2,5-diphenyl-2-H-tetrazolium bromide) assay. There was no significant decrease in cell viability after co-culture with Blank@NP or PSB@NP-FA at different concentrations for 24 or 48 h (Figures S4A and S4B), even up to 400 μg/mL, indicating the good biosafety of PLGA-based Blank@NP and PSB@NP-FA *in vitro*.

To assess the biocompatibility of Blank@NP *in vivo*, the mice were intravenously administered daily with Blank@NP at a dose of 30 mg/kg for 7 days. By measuring weight changes on a daily basis, the results showed that there was no significant weight loss within 7 days compared with untreated control mice (Figure S4C). At the end of the experiment, the blood was collected for hematological and biochemical analyses, and the major organs (heart, liver, spleen, lung, and kidney) for H&E staining. The hematological or biochemical parameters results showed that Blank@NP-treated mice were consistent with those of the control mice (Figure S5A). Histological sections also showed no pathological changes in organs in both Blank@NP-treated mice and control mice (Figure S5B), indicating the excellent biocompatibility of Blank@NP *in vivo*.

PSB@NP-FA alleviates DSS-induced acute colitis

The anti-oxidant and anti-inflammatory properties of PSB@NP-FA and the capability of ROS-responsive drug release made it promising for clinical application. We then used DSS-induced mice colitis to verify its anti-inflammatory activity further, and the experimental design illustration is shown in Figure 4A. It was found that the body weight of DSS group mice decreased significantly from the third day and decreased sharply from the fifth day. In contrast, the PSB@NP-FA-treated group prevented the body weight loss to some extent (Figure 4B), indicating that PSB@NP-FA was helpful in the treatment of UC. In addition to changes in body weight, the disease activity index (DAI) including stool consistency and fecal occult blood was also analyzed. As shown in Figure 4C, compared with the DSS group, the DAI of mice in the PSB@NP-FA group increased slowly, and the effect in the 30 mg/kg of PSB@NP-FA-treated group was the best. The colon length also showed that the colon in DSS group mice was significantly shortened ($p < 0.01$) and recovered to a certain extent after PSB@NP-FA treatment (Figures 4F and 4G). Glutathione (GSH) is an important anti-oxidant in the body, which is also an important indicator to measure the anti-oxidant capacity of drugs. The content of GSH in the colon of the healthy control group was as high as 19 μM/g protein, and in the DSS group decreased significantly (Figure 4D). After treatment with PSB@NP-FA, the content of GSH increased in a dose-dependent manner,

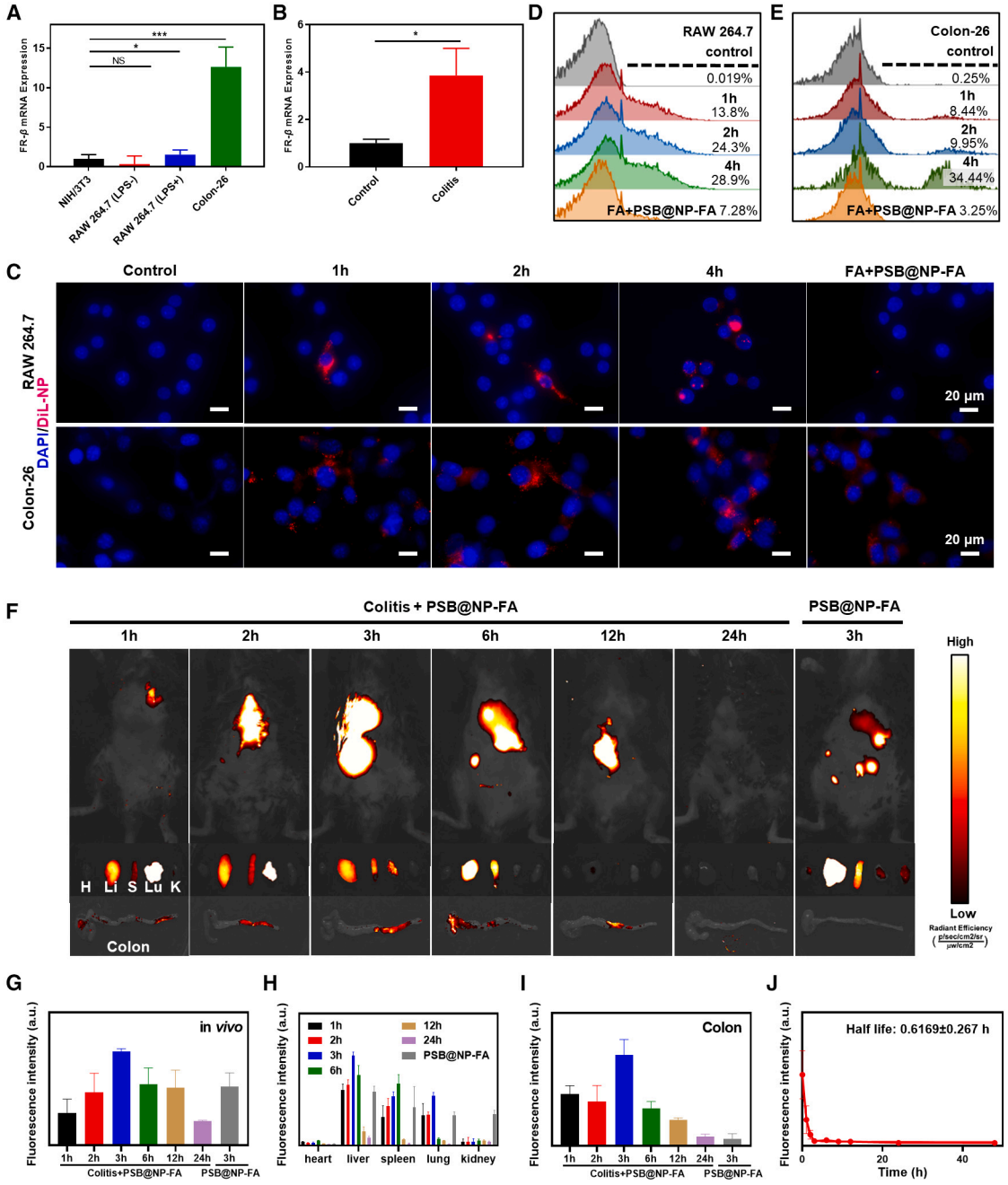

Figure 3. Evaluation of the targeting ability of PSB@NP-FA both *in vivo* and *in vitro*

(A) FR-β mRNA expression in different cell lines. (B) FR-β mRNA expression in the colon of healthy control mice and DSS-induced colitis mice. (C) DiL-labeled PSB@NP-FA were efficiently internalized by RAW 264.7 cells and Colon-26 cells. Here, NPs were labeled by DiL (red) and nucleus was stained by DAPI (blue). Scale bar, 20 μm. (D) Cellular uptake efficiency of NP by RAW 264.7 cells was quantified by flow cytometry. (E) Cellular uptake efficiency of NP by Colon-26 cells was quantified by flow cytometry. (F) Fluorescence images of healthy mice and DSS-induced colitis mice, organs, and colon tissues at indicated time points after intravenous injection of PSB@NP-FA. (G) Quantification of the fluorescence intensity *in vivo*. (H) Quantification of the fluorescence intensity of major organs. (I) Quantification of the fluorescence intensity of colon tissues. (J) Pharmacokinetics of PSB@NP-FA in DSS-induced colitis mice.

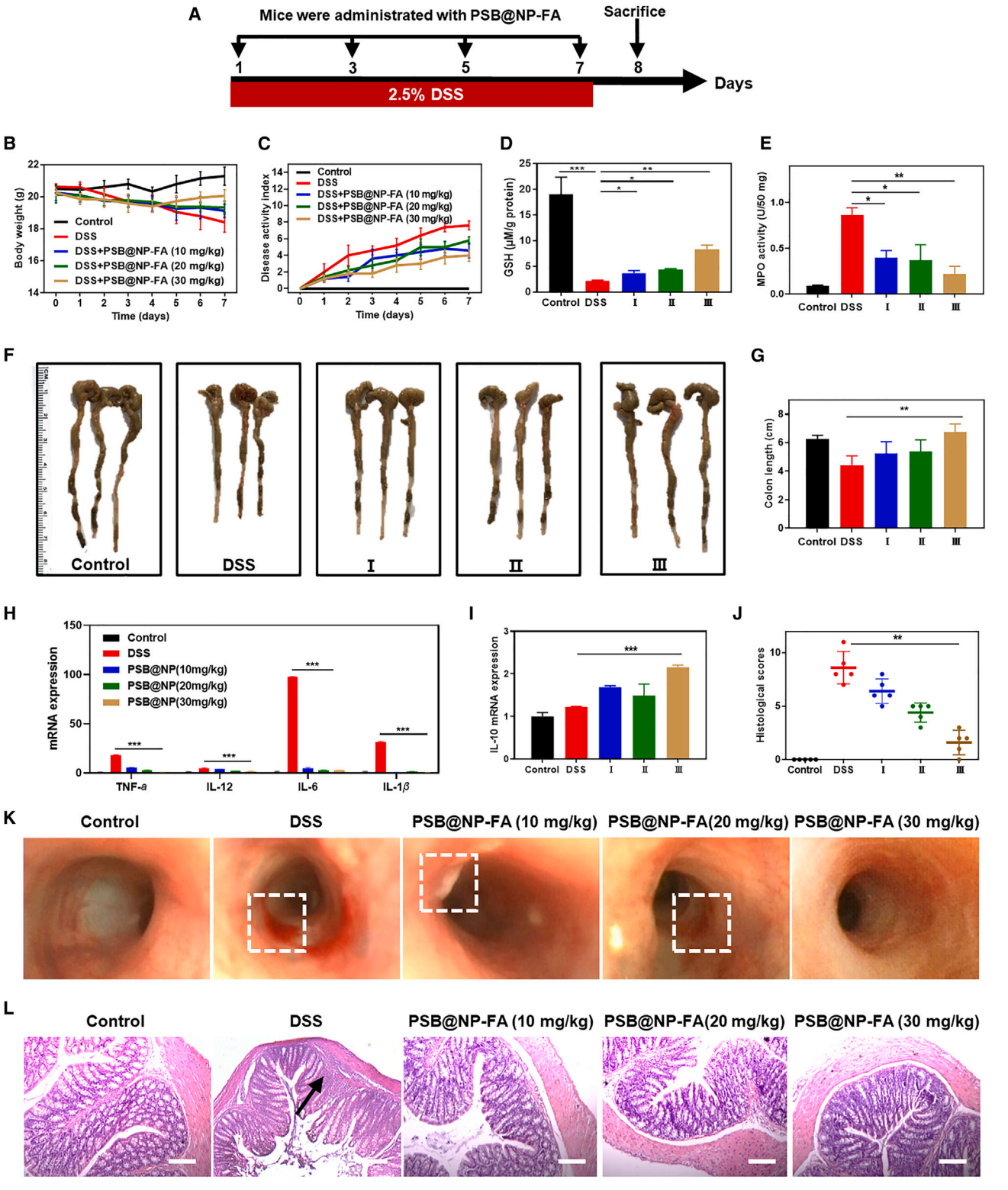

(legend on next page)

with the highest increase at the dose of 30 mg/kg (Figure 4D). Moreover, Figure 4E shows that myeloperoxidase (MPO) activity increased in the DSS group, indicating inflammation and a large amount of MPO secreted by neutrophil infiltration. In contrast, PSB@NP-FA treatment reduced inflammation, as demonstrated by MPO activity, but only PSB@NP-FA-treated groups (30 mg/kg) exhibited a marked decrease. To evaluate the anti-oxidant capacity of PSB@NP-FA *in vivo*, we used frozen sections of the colon of each group of mice and detected the fluorescence intensity with ROS probe DCFH-DA to reflect the content of ROS in the colon tissues. The results in Figure S6A showed that there was almost no fluorescence signal in healthy tissues except for the spontaneous fluorescence in the muscular layer, while the fluorescence signal in the DSS group was significantly enhanced, indicating the production of a large number of ROS in the tissues. After treatment with PSB@NP-FA, fluorescence intensity decreased in a dose-dependent manner, reflecting the decrease of ROS content in the colon. The intensity of the fluorescence signal in each group was calculated by ImageJ and displayed as a histogram (Figure S6B).

The results of inflammatory factors showed that the expression levels of pro-inflammatory factors (TNF-α, IL-6, IL-12, and IL-1β) in the DSS-treated group were significantly upregulated compared with the control group ($p < 0.01$) (Figure 4H). When treated with PSB@NP-FA at different concentrations, the expression level of TNF-α, IL-6, IL-12, and IL-1β was significantly decreased compared with the DSS group, while the expression of anti-inflammatory factor IL-10 was increased (Figure 4I).

Additionally, endoscopic images showed a reduction in the number of ulcers in the colonic mucosa of PSB@NP-FA-treated mice (30 mg/kg) (Figure 4K). In contrast, inflammation remained severe in the DSS group, with extensive redness and ulcers (Figure 4K). Results with PSB@NP-FA (10 mg/kg or 20 mg/kg) offered lower efficacy. Histological staining with H&E was used to observe the injury and lesion of colon tissue, and the differences among groups were statistically analyzed by histological scores. Results showed that the colonic mucosa of healthy mice in the control group was intact, and the crypt was apparent (Figure 4L). In contrast, crypts disappeared, and neutrophils infiltrated in colonic tissues of mice with colitis (Figure 4L). Compared with the DSS group, the colonic tissue of the PSB@NP-FA treatment group recovered, and the morphology was similar to that of the healthy control group. The histological scores were obtained, and the results showed that the histological score in the DSS group was much higher than the PSB@NP-FA-treated groups; the histological score significantly decreased after PSB@NP-FA treatment and gradually returned to the healthy level in a dose-dependent manner, with the lowest score at the dose of 30 mg/kg (Figure 4J). The above results indicated that PSB@NP-FA had a good scavenging capacity of ROS and anti-inflammatory activity, and could effectively relieve DSS-induced colon inflammation in mice.

PSB@NP-FA relieves colonic inflammation by regulating DCs and colonic M1/M2 macrophage polarization

Dendritic cells (DCs) and macrophages are two kinds of cells mainly involved in innate immune responses. DCs are antigen-presenting cells, and their dysfunction is the main cause of UC.[41] DCs from the intestinal tract can not only promote the activation of T cells but also induce T cells to move toward the intestinal tract, and the interaction between DCs and T cells can induce immune responses. Intestinal intraepithelial lymphocytes (IELs) are located in the basal layer of intestinal epithelial cells and maintain intestinal homeostasis. We observed that the number of DCs in IELs decreased significantly after PSB@NP-FA treatment (Figures 5A and S7), and the proportion of DCs in LPL in each group did not change significantly (Figures 5B and S8). However, the number of DCs in the DSS group increased significantly, and decreased significantly after PSB@NP-FA treatment (Figure 5C). The results showed that, in the DSS-induced colitis model, DCs were involved in initiating intestinal mucosal immune responses, and the PSB@NP-FA restored the intestinal immune homeostasis, possibly due to changes in the number and function of DCs.

According to their functions and secretory factors, macrophages can be divided into classically activated M1 phenotype macrophages and selectively activated M2 macrophages. M1 phenotype macrophages mainly secrete pro-inflammatory factors and play an important role in the early stage of inflammation. M2 phenotype macrophages express anti-inflammatory cytokines and play a role in inhibiting the inflammatory response and tissue repair. We further examined the effects of PSB@NP-FA on macrophage polarization. A strong M1 response occurred in the colon in the DSS-induced model, which was represented by an increase in the number of M1 in LPLs and the percentage of M1 in LPLs (Figures 5D and 5E). However, as shown in Figure 5F, the proportion of M2 phenotype macrophages in LPL decreased. After administration with PSB@NP-FA, the percentage of M1 phenotype macrophages significantly reduced, and the percentage of M2 phenotype in LPLs remarkably increased compared with the DSS group (Figures 5D–5F). Flow cytometry results reflected changes in the proportion of M1 and M2 macrophages in LPLs and showed that DSS could increase the percentage of M1 phenotype macrophages, which could be effectively reduced after PSB@NP-FA treatment (Figure 5G). The percentage of M2 phenotype macrophages in LPLs decreased after DSS induction but increased after

Figure 4. PSB@NP-FA alleviates DSS-induced acute colitis

(A) Illustration of the experimental design. (B) Bodyweight loss. (C) DAI scores. (D) The content of GSH. (E) MPO activity. (F) Photographs of the excised colons in different groups. (G) Colon length. (H) The mRNA levels of pro-inflammatory factors (TNF-α, IL-6, IL-12, and IL-1β) in colon tissues (n = 3). (I) The mRNA levels of IL-10 in colon tissues (n = 3). (J) Histological score of H&E sections. (K) Endoscopic images of colons. The dotted boxes represented ulcers and inflammation. (L) H&E staining of colonic sections. Arrows indicated neutrophil infiltration. Scale bar, 20 μm. The symbol I stands for DSS+PSB@NP-FA(10 mg/kg), II stands for DSS+PSB@NP-FA(20 mg/kg), III stands for DSS+PSB@NP-FA(30 mg/kg).

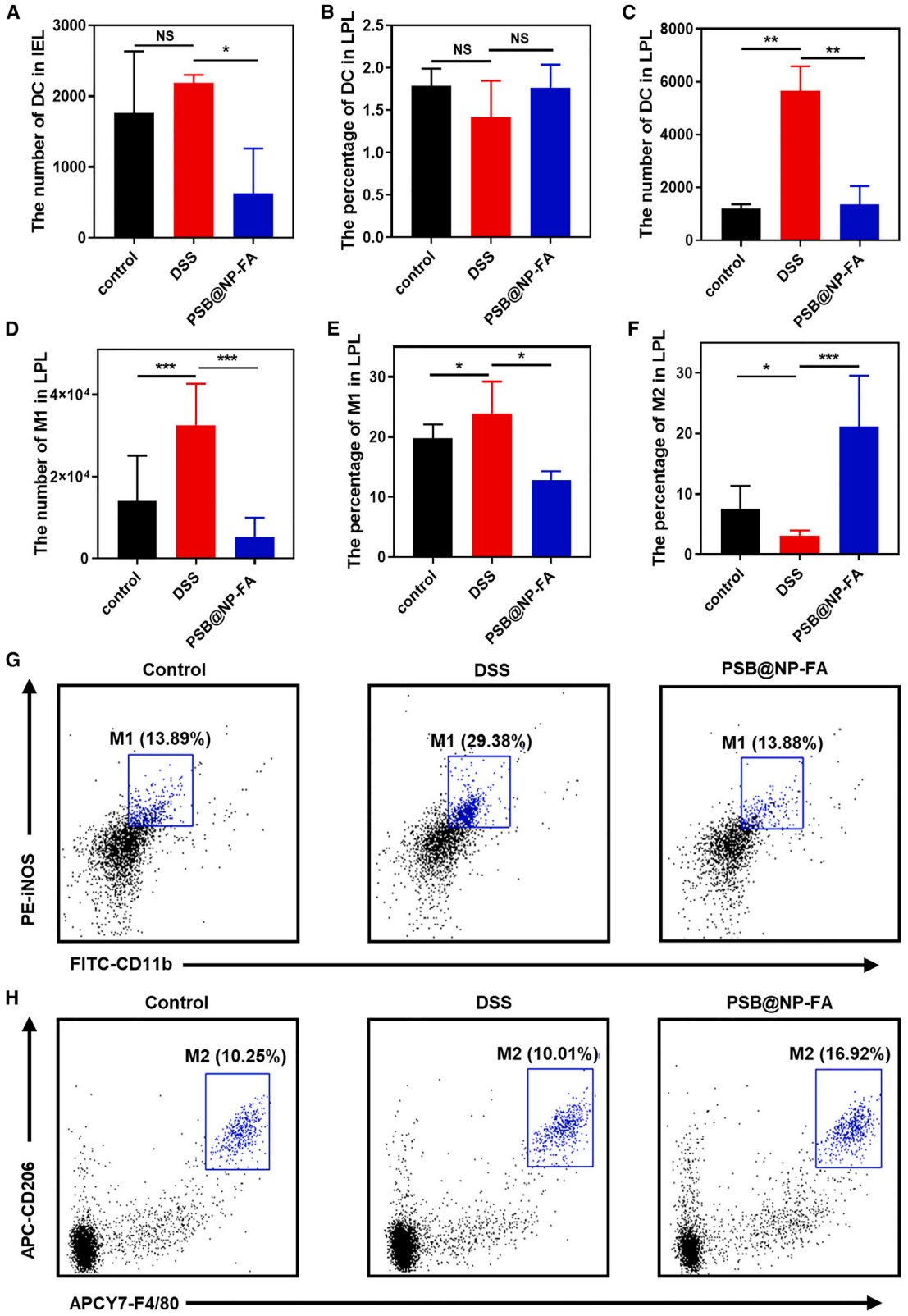

(legend on next page)

being administrated with PSB@NP-FA (Figure 5H). These results suggested that PSB@NP-FA promotes the macrophage phenotypic switching from an inflammatory M1 phenotype to an alternatively activated M2 phenotype, which is beneficial for the remission of colonic inflammation.

PSB@NP-FA reduces colonic inflammation by regulating T cell infiltration

To identify the therapeutic effect of PSB for UC is through the regulation of T cell infiltration, flow cytometry was used to measure the T cell profile in LPLs and IELs. After DSS-induced colitis in mice, the number of IELs changed significantly (Figure 6A), suggesting that the disorder of IELs is related to inflammation. As shown in Figure 6B, the total number of activated cells in LPLs increased in the DSS group, but decreased significantly in the PSB@NP-FA group, suggesting that PSB@NP-FA has an effective immunomodulatory effect on DSS-induced colitis in mice.

Regulatory T cells (Treg) are a subset of $CD4^+$ T cells with significant immunosuppressive effects, which can inhibit the immune responses of other cells and play an important role in maintaining the immune balance of the body. The proportion of Treg cells in the DSS group was increased, but there was no statistical significance (Figures 6C and S9). The number of Treg cells was significantly increased in the DSS group but was significantly decreased in the PSB@NP-FA group (Figure 6D), suggesting that PSB@NP-FA may play an anti-inflammatory role in alleviating UC by regulating Treg cell subsets.

Several studies have shown that $CD4^+$ T cells are closely related to the pathogenesis of UC.[11,42] According to the expression of CD45RA and CCR7, the majority phenotype of $CD4^+$ T cells could be divided into central memory T cell (TCM), effect T cell, and T-naive groups. The results showed that the percentage of $CD4^+$ T cells in LPLs increased in mice with colitis but decreased after PSB@NP-FA treatment (Figures 6E and S10). The other three main phenotypes of CD4+ T cells also changed in different groups (Figures 6F–6H and S11). In terms of cell number, $CD4^+$ T cells in LPLs significantly increased in colitis mice, but it could be effectively reversed by PSB@NP-FA (Figures 6I–6L). The same results were observed in $CD8^+$ T cells in LPLs (Figures 6M, 6N, and S12). The proportion of $CD8^+$ T cells in IELs did not change significantly, but the number decreased in both the DSS group and PSB@NP-FA group (Figures 6O, 6P, and S13), indicating that $CD8^+$ T cells in IELs were also involved in the immune response process.

Furthermore, the proportions of the secretion of cytokines (interferon gamma [IFN-γ], IL-17, and TNF-α) in $CD4^+$ T cells were not significantly different among the three groups (Figures 7A–7C and S14), but the number was significantly increased in the DSS group (Figures 7D–7F). Compared with the DSS group, the number of IFN-γ, IL-17, and TNF-α were decreased in the PSB@NP-FA group (Figures 7D–7F), indicating a significant decrease in the number of $CD4^+$ T cytokine-secreting cells. Moreover, there was no statistical difference in the proportion of $CD8^+$ T cytokines (IFN-γ, IL-17, and TNF-α) in LPLs (Figures 7G–7I), but the number increased significantly in the DSS group and could be reversed by the PSB@NP-FA group (Figures 7J–7L). These results suggested that T cells infiltrated in colitis, and the alleviating effect of PSB@NP-FA on UC was achieved by regulating T cells.

The combination of the PSB and DEX enhances the therapeutic efficacy of colitis

DEX, a corticosteroid, is one type of medication that may be prescribed to treat inflammation of the gastrointestinal tract. DEX is used as a short-term treatment for Crohn's disease and UC because it reduces inflammation quickly. The nano-delivery platform with fewer doses can achieve a similar therapeutic effect to free DEX, and targeted delivery avoids systemic toxic side effects. Because of the good therapeutic effect of PSB@NP-FA on UC, we next evaluated whether the combination of the PSB and DEX could enhance the therapeutic efficacy of colitis. First, we synthesized DEX/PSB@NP-FA, which is spherical in shape (Figure S15A), with a particle size of 190.14 nm (Figure S7B) and a potential of −28.11 mV (Figure S15C). The entrapment efficiency and LC% of DEX were 64.69% and 9.51%, respectively (Figures S15D and S15E), and it had sustained release characteristics (Figures S15F). After establishing the UC model, free DEX, PSB@NP-FA, and DEX/PSB@NP-FA were used to treat colitis mice. As expected, body weight loss, DAI level, and MPO activity were high in the DSS group (Figures 8A–8C). In contrast, by being treated with free DEX, PSB@NP-FA, and DEX/PSB@NP-FA, they effectively attenuated body weight loss and DAI as well as MPO activity (Figures 8A–8C). Among them, the DEX/PSB@NP-FA group had the best anti-inflammatory effect. By observing the colonic tissue and mesenteric lymph nodes of each group, it was found that DSS successfully induced colitis, specifically manifested as colon shortening and mesenteric lymph node hyperplasia (Figure 8D). DEX/PSB@NP-FA could effectively restore colon length and relieve mesenteric lymph nodes (Figure 8D). Statistical results of colon length are shown in a histogram (Figure 8E). In addition, the expression of pro-inflammatory factors (TNF-α, IL-1β, IL-6, and IL-12) in colon tissues of the DSS group was higher than that of the healthy group ($p < 0.05$) (Figure 8F). The levels of TNF-α, IL-1β, IL-6, and IL-12 in PSB@NP-FA, free DEX, or DEX/PSB@NP-FA treatment groups significantly reduced, among which the lowest level was the DEX/PSB@NP-FA group (Figure 8F). The expression level of IL-10 also increased in the treatment group

Figure 5. PSB@NP-FA relieves colonic inflammation by regulating DCs and colonic M1/M2 macrophage polarization

(A) The number of DCs in IEL. (B) The percentage of DCs in LPLs. (C) The number of DCs in LPLs. (D) The number of M1 phenotype macrophages in LPLs. (E) The proportion of M1 phenotype macrophages in LPLs. (F) The proportion of M2 phenotype macrophages in LPLs. (G) Representative image of the proportion of M1 in LPLs shown by flow cytometry. (H) Representative image of the proportion of M2 in LPLs demonstrated by flow cytometry. Representative scatterplots of flow cytometry are provided in the supplemental information.

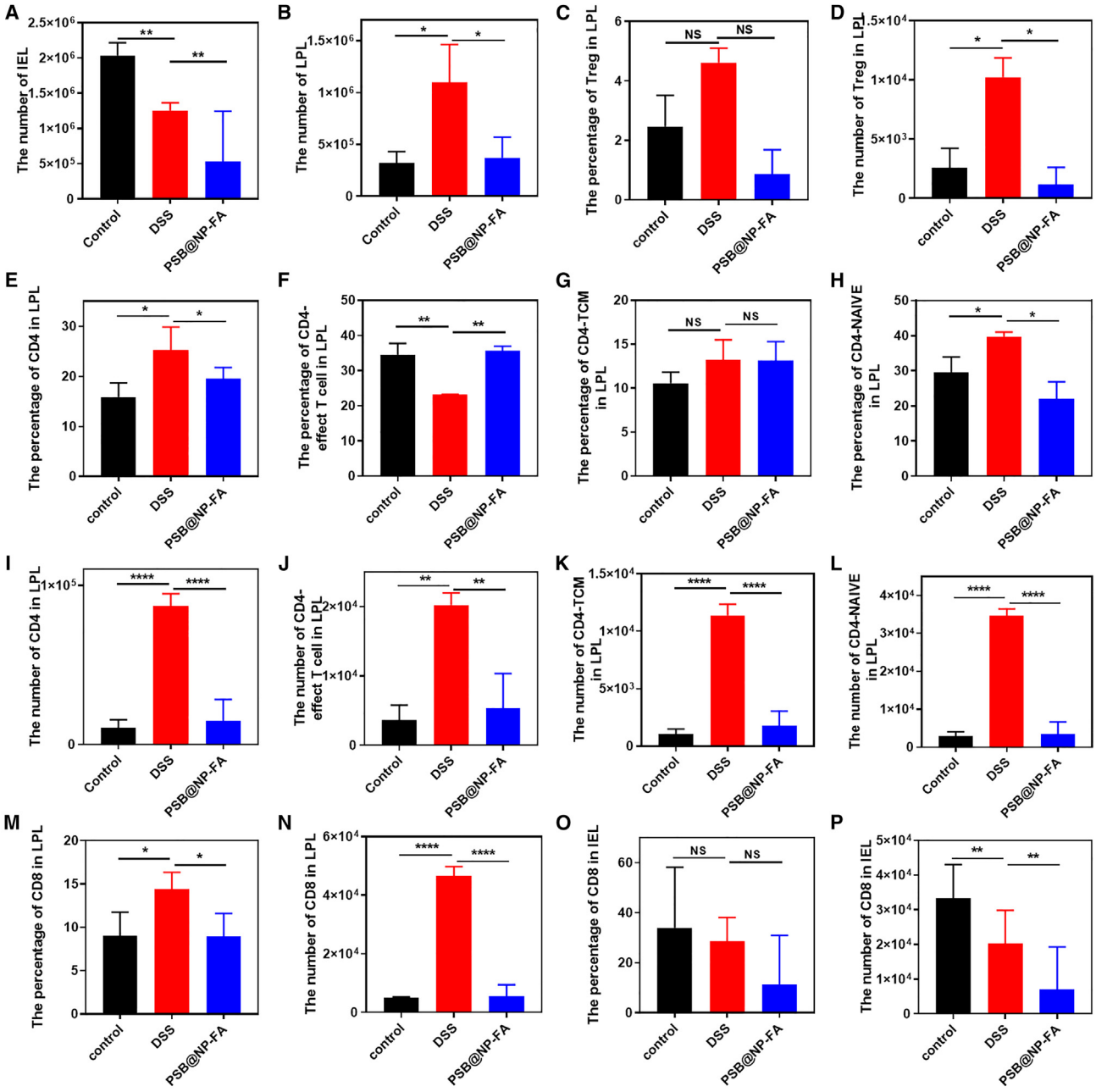

Figure 6. PSB@NP-FA reduces colonic inflammation by regulating T cell infiltration

(A) The number of cells in IELs. (B) The number of cells in LPLs. (C) The percentage of Tregs in LPLs. (D) The number of Tregs in LPLs. (E) The percentage of $CD4^+$ T cells in LPLs. (F) The percentage of $CD4^+$ T cells-effect T cell in LPLs. (G) The percentage of $CD4^+$ T cells-TCMs in LPLs. (H) The percentage of $CD4^+$ T cells naive in LPLs. (I) The number of $CD4^+$ T cells in LPLs. (J) The number of $CD4^+$ T cells-effect T cell in LPLs. (K) The number of $CD4^+$ T cells-TCMs in LPLs. (L) The number of $CD4^+$ T cells naive in LPLs. (M) The percentage of $CD8^+$ T cells in LPLs. (N) The number of $CD8^+$ T cells in LPLs. (O) The percentage of $CD8^+$ T cells in IELs. (P) The number of $CD8^+$ T cells in IELs. Representative scatterplots of flow cytometry are provided in the supplemental information.

(Figure 8G), indicating the therapeutic effect on murine colitis. H&E staining sections showed that free DEX, PSB@NP-FA, or DEX/PSB@NP-FA reversed colon damage, and the DEX/PSB@NP-FA had the best protective effect on colon epithelial cells compared with the free DEX (Figure 8H). Taken together, these results showed that DEX/PSB@NP-FA achieved a better therapeutic effect than free DEX at a much lower dose and accelerated the recovery of the impaired intestinal mucosa in UC therapy.

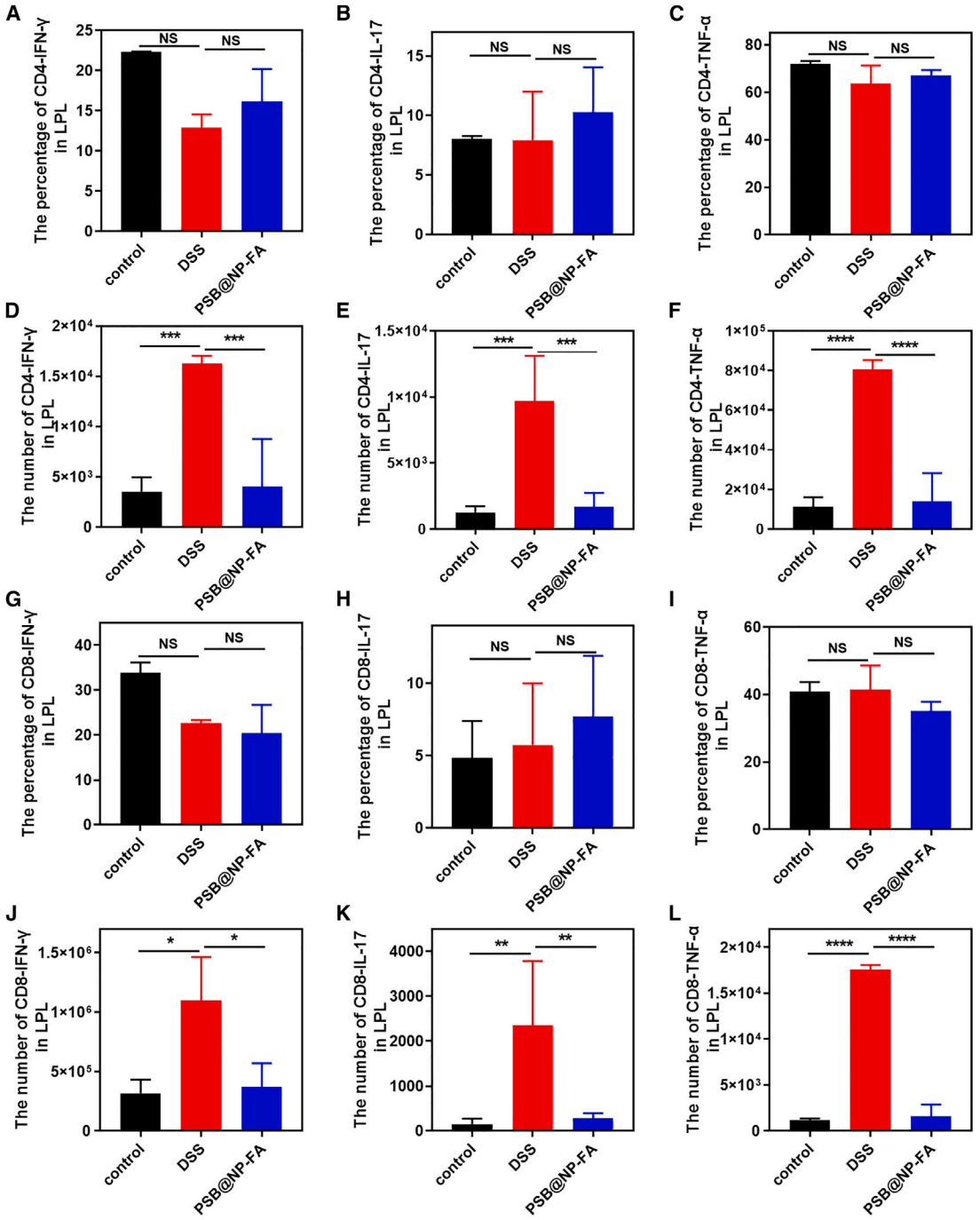

Figure 7. The number and percentage of cytokines secreted by CD4⁺ and CD8⁺ T cells

(A) The percentage of CD4⁺ T cells-IFN-γ in LPLs. (B) The percentage of CD4⁺ T cells-IL-17 in LPLs. (C) The percentage of CD4⁺ T cells-TNF-α in LPLs. (D) The number of CD4⁺ T cells-IFN-γ in LPLs. (E) The number of CD4⁺ T cells-IL-17 in LPLs. (F) The number of CD4⁺ T cells-TNF-α in LPLs. (G) The percentage of CD8⁺ T cells-IFN-γ in LPLs. (H) The percentage of CD8⁺ T cells-IL-17 in LPLs. (I) The percentage of CD8⁺ T cells-TNF-α in LPLs. (J) The number of CD8⁺ T cells-IFN-γ in LPLs. (K) The number of CD8⁺ T cells-IL-17 in LPLs. (L) The number of CD8⁺ T cells-TNF-α in LPLs. Representative scatterplots of flow cytometry are provided in the supplemental information.

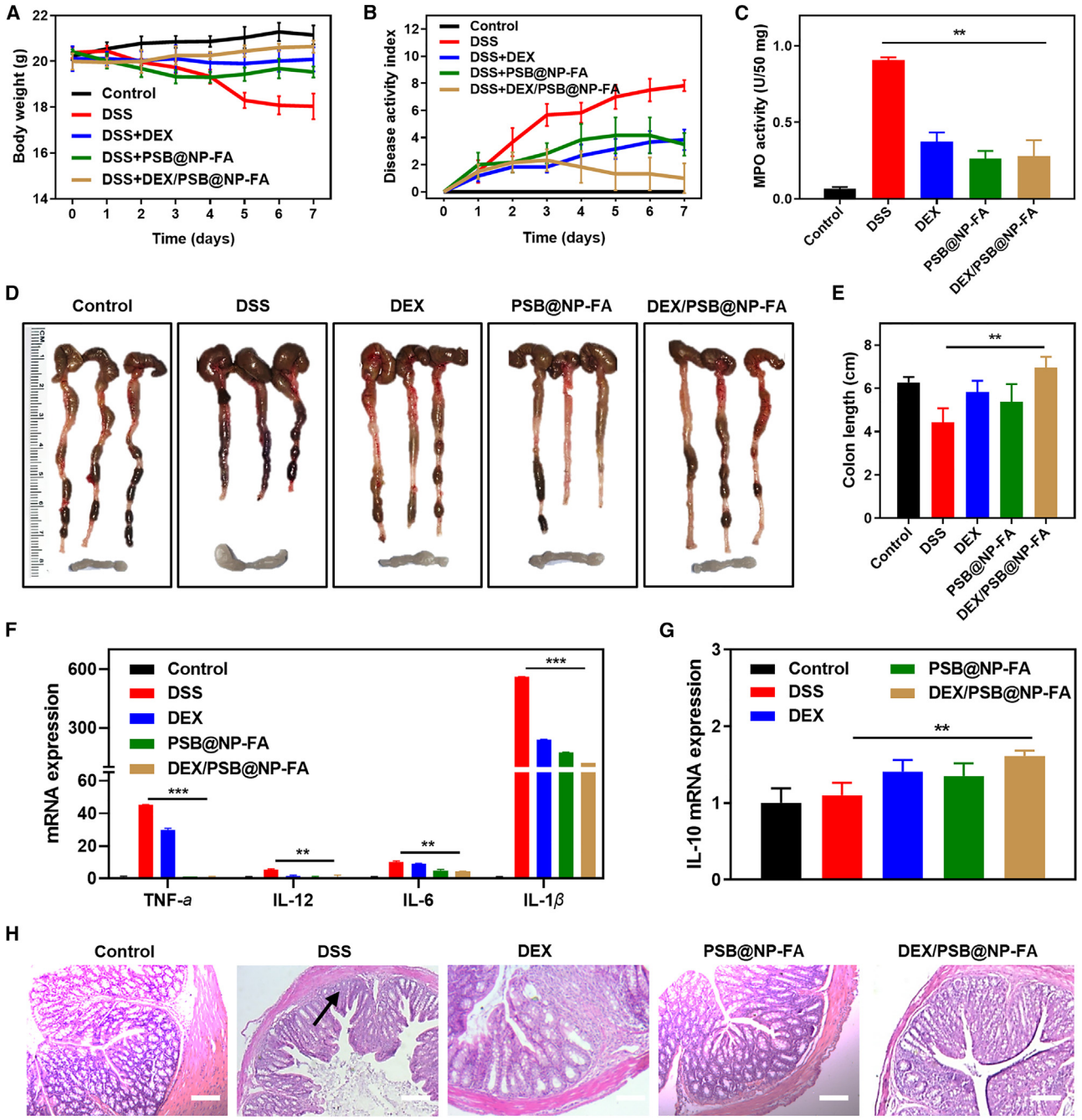

Figure 8. The combination of the PSB and DEX enhances the therapeutic efficacy of colitis

(A) Body weight (n = 6). (B) DAI scores. (C) MPO activity. (D) Colons and mesenteric lymph nodes. (E) Colon length. (F) The mRNAs expression of TNF-α, IL-12, IL-6, and IL-1β in different groups (n = 3). (G) The mRNA expression of IL-10 in different groups (n = 3). (H) H&E staining of colonic sections among different groups. Scale bar, 20 μm.

DISCUSSION

PSB relieved a series of symptoms of DSS-induced colitis in mice, such as changes in inflammatory factors, decreased DAI, and histological morphology by modulating macrophage phenotypic and the infiltrations of immune cells. It is worth noting that PSB was known as the second generation of resveratrol. Notably, as a dimethylated analogue of resveratrol, PSB and resveratrol exhibited many pharmacological similarities. PSB had a higher bioavailability than resveratrol because of two methoxy groups, which increased lipophilic and oral absorption.[43–45] Therefore, PSB was more biologically active than

resveratrol in anti-inflammatory and anti-oxidant activity. Moreover, a low oral dose of PSB was beneficial to cognitive function,[46] and dietary PSB could effectively prevent intestinal-related diseases.[47,48] Still, the mechanism of PSB remained to be further studied.

Receptors, such as CD98, CD44, and FRs, are highly expressed on colonic cells during UC, which provides a potential strategy for targeted modification of NPs. Recent studies have shown that hyaluronic acid-modified bilirubin NPs can target macrophages in the inflammatory site and treat UC by regulating innate immunity.[49] Polymer NPs loaded with HSP90 could target the inflamed colon via FA ligand, which enhanced cell internalization efficiency, and increased the drug concentration in the colon to alleviate UC.[50]

Particle size plays an important role in targeting ability and cell internalization. The loose arrangement of cells in inflammatory tissues and the increased vascular permeability makes it easier for smaller NPs to accumulate in inflammatory sites preferentially. The particle size of the PSB@NP-FA is about 200 nm, which is excellent for targeted drug delivery. In addition to passive targeting, it can also actively target the colon to effectively scavenge ROS in colon tissues and play an anti-inflammatory and anti-oxidant role.

ROS are closely associated with the pathological process of UC. A large number of immune cells infiltrate the inflamed colon tissue in the pathological process of UC, producing a large amount of ROS, inducing cell oxidative stress damage, and exacerbating the inflammatory response. H_2O_2 is one of the most common endogenous ROS. In this work, a ROS-responsive (thioketal linkage), FA-functionalized nanocarrier for efficient PSB delivery (PSB@NP-FA) to the inflamed colon was designed. It is generally believed that the physiological concentration of H_2O_2 in normal cells is about 10 nM and that in inflammatory tissue cells is more than 100 mM.[51,52] In this study, concentrations of H_2O_2 ranging from 10 μM to 10 mM were used to demonstrate the ROS-responsive property of PSB@PLGA-TK-PEG (PSB@NP-FA). With ROS-responsive and ROS-scavenging properties, PSB@NP-FA could break down and release the encapsulated PSB when it reached the site of high expression of ROS in colon inflammation, thereby protecting RAW 264.7 cells from H_2O_2-induced oxidative damage.

In this study, the PSB dose (10, 20, and 30 mg/kg/day) was selected for the UC model. PSB@NP-FA with 30 mg/kg treatment showed more decisive anti-inflammatory action with the lowest body weight loss, the most extended colon length, and the lowest DAI. In contrast, PSB@NP-FA with 10 mg/kg treatment did not perform well in most results. These results suggested that the anti-inflammatory action of PSB@NP-FA was dose dependent, and the dosage in the animal model should be optimized. In addition, DEX/PSB@NP-FA achieved a similar therapeutic effect in a lower dose compared with the free DEX, which is one of the advantages of NPs.

T lymphocytes play an important regulatory role in the immune system and widely exist in the normal intestinal mucosa.[53–55] Among them, 60%∼70% of T cells in intestinal lamina propria are $CD4^+$ T cells.[56,57] Dysregulation of $CD4^+$ T cells might lead to a variety of autoimmune diseases and inflammatory diseases,[58,59] which was proved by our experiment. We found that the total number of $CD4^+$ T cells and related cells secreting cytokines decreased in LPLs, thus confirming the involvement of $CD4^+$ T cells in regulating colonic mucosal immunity. Its lack might be an important factor in the pathogenesis of UC. IFN-γ was one of the most abundant pro-inflammatory cytokines produced by $CD4^+$ T cells in the mucous membrane of patients with UC, which was secreted by Th1 and Th17 cells. The decrease of IFN-γ in UC also supported this conclusion. However, it was not clear whether the differentiation state of $CD4^+$ T cells affects the development and remission of chronic inflammatory and autoimmune diseases, and the interaction mechanism between $CD4^+$ T cells and macrophages also needs to be further studied.

It was shown that remission of murine colitis was achieved by intervening immune responses. However, the number of IELs was not reversed after PSB@NP-FA treatment (Figure 7A), which may be due to the fact that IELs were divided into two subgroups, natural IELs and induced-type IELs. Induced-type IEL was a kind of cytotoxic T cell and the specific classification of which type is dominant needs further investigation. Moreover, the proportion of $CD8^+$ T cells in IELs did not change significantly (Figure 7O), but the number of cells decreased in the DSS group and did not reverse this result in the PSB@NP-FA group (Figure 7P), which may be due to the large difference in the total number of cells in IELs among the three groups.

Generally speaking, T cells changed little at day 8 of inflammation in many studies, but $CD4^+$ T cells in LPL in the DSS group changed significantly in our results. This may be because the total number of LPL cells in the DSS group is much higher, so the proportion of $CD4^+$ T cells is correspondingly much higher. In addition, unactivated naive cells account for the largest proportion of $CD4^+$ T cells, up to 40%. Therefore, most naive $CD4^+$ T cells only migrate to the inflammatory site of the colon but have not yet been involved in the local immune response. In addition, DCs and macrophages, which were mainly involved in the innate immune response, accounted for a large proportion of the cell subsets, and $CD4^+$ T cells and $CD8^+$ T cells were also involved, indicating that the DSS-induced murine colitis model includes both innate and adaptive immune responses.

In summary, we designed a nanocarrier-loading PSB (PSB@NP-FA) with ROS-responsive capability via thioketal linkage and realized the controlled PSB release to alleviate UC. PSB@NP-FA showed excellent ROS-scavenging, ROS-responsive properties, and anti-inflammatory effects *in vitro*. PSB@NP-FA could be efficiently internalized by Colon-26 cells and RAW 264.7 cells and preferentially localized to the inflamed colon by intravenous administration. In the colitis model, PSB@NP-FA could efficiently relieve UC by regulating DCs and colonic M1/M2 macrophage polarization (two kinds of cells mainly involved in innate immune responses) and T cell infiltration (involved in adaptive immune responses). More

importantly, the combination of the PSB and DEX could enhance the therapeutic efficacy of colitis. With dependable biocompatibility, this nanocarrier represents an alternative therapeutic approach to UC, and it can also be used as a synergist for classic anti-inflammatory drugs of UC.

MATERIALS AND METHODS

Materials

Lactide: glycolide (50:50) (PLGA, wt: 38,000∼54,000), poly(vinyl alcohol) (PVA, 86%–89% hydrolyzed, low molecular weight), FA-SH, and PLGA-TK-PEG-COOH were obtained from Ruixi Biological Technology (Xi'an, China). PSB and DEX were from Meilun Bio (Dalian, China). PLGA-PEG-Mal (PEG MW 5000) was acquired from NSP-Functional polymers and copolymers (Winston-Salem, USA). Fluorescent dyes (DiL and DiR) were obtained from Promokine (Heidelberg, Germany).

Design, preparation, and characterization of a ROS-responsive NP

The Blank@NP, PSB@NP, and DEX/PSB@NP were prepared using a versatile single-step surface-functionalizing technique described in our previously published work.[34] PLGA, PLGA-PEG-Mal, and PLGA-TK-PEG-COOH (a ROS-responsive polymer) were used as polymers to load drugs. PSB, DEX, and the polymers mentioned above were dissolved in dichloromethane (DCM, 2 mL) with a specific proportion. An oil-in-water emulsion was formed by emulsifying the polymer solution in 4 mL of 2.5% w/v aqueous PVA solution drop by drop. Then a probe sonicator was used at 25% amplitude for 4 min (Branson S-450; Danbury, USA) on an ice bath followed by 0.5 h of vacuum evaporation with a rotary evaporator to remove the residual DCM. The emulsion was stirred overnight at room temperature. NPs were recovered by centrifugation and washed with deionized water three times. NPs suspension was then lyophilized to obtain a dry powder and then the entrapment efficiency and LC% of PSB in NPs was measured by UV-vis spectrophotometer (U-3310, Hitachi, Japan). The calculated formulas were as follows:

Entrapment efficiency (%) = weight of encapsulated drug/weight of drug added × 100%

LC% = weight of encapsulated drug/weight of NPs × 100%

FA was then chosen to conjugate with NPs through the Michael addition reaction between the maleimide moiety in PLGA-PEG-Mal and the sulfhydryl group in FA-SH. The product was subsequently characterized by FTIR spectrometry. Infrared spectra were recorded as neat samples on a PerkinElmer FTIR spectrometer (100S).

The particle size, polydispersity index, and zeta potential of the PSB@NP were measured using a Zetasizer Nano-ZS90 (Malvern, UK) at room temperature. TEM was used to measure the morphology of the NPs, 5 μL of NPs solution was dripped onto the carbon-coated copper TEM grid for 5 min, then the NPs were negatively stained by phosphotungstic acid before TEM characterization.

In vitro ROS-responsive release study

PSB@PLGA-TK-PEG were placed into a membrane of a molecular weight cutoff of 10 kDa using the dialysis method and dialyzed separately in PBS solutions (pH 6.8 and pH 7.4) with or without 10 μM H_2O_2 at 37°C under shaking at 100 rpm. For comparison, PSB@PLGA was used as a control group. The concentration of NP in the dialysis bag was 1 mg/mL with 5 mL in total. The volume of the released media outside the dialysis bag is 50 mL. At the scheduled times, 3 mL of released media was collected, and the same amount of fresh dialysis fluid was added. Finally, a UV-vis spectrophotometer was used to measure the PSB concentrations in the released media.

Determination of ROS-scavenging capability of PSB@NP

To evaluate the H_2O_2-scavenging capacity of PSB@NP, different concentrations of PSB@NP or free PSB were incubated with varying concentrations of H_2O_2 for 20 min. A fluorimetric hydrogen peroxide assay kit (MAK165, Sigma-Aldrich) was used to measure the concentration of residual H_2O_2.

To study the protective effect of PSB@NP on cells from oxidative stress damage, RAW 264.7 macrophages were incubated overnight in 24-well plates at a concentration of 1×10^5 cells/well. After cell adherence, the medium was removed and replaced with a medium containing PSB@NP (200 μg/mL) or free PSB (equal to PSB@NP) and co-incubated for another 24 h. After removing the medium, cells were washed with PBS twice and then added to the medium containing 100 μM H_2O_2. Cell viability was detected by MTT assay.

To evaluate the anti-oxidant capacity of PSB@NP *in vivo*, we used frozen sections of the colon of each group of mice and detected the fluorescence intensity with ROS probe DCFH-DA (Beyotime, China) to reflect the content of ROS in the colon tissues.

In vitro anti-inflammatory effect of PSB@NP

RAW 264.7 cells were seeded in 24-well plates with a concentration of 1×10^5 cells/well. After cell adherence, the control group was replaced with a fresh medium, and different NPs were added into the medium of the experimental groups. After the NPs were incubated with RAW 264.7 cells for 6 h, 500 ng/mL of LPS was added to induce inflammation. Subsequently, cells were collected and isolated of total RNA, whereas the levels of inflammatory cytokines (TNF-α, IL-6, IL-12, IL-1β, and IL-10) were quantified by qRT-PCR. The primers are listed in Table S1.

In vitro cellular uptake assay

Cellular uptake and intracellular distributions of DiL-labeled PSB@NP-FA in RAW 264.7 and Colon-26 cells were visualized by confocal microscopy. For the experiment, cells were cultured on glass plates and then incubated with DiL-labeled PSB@NP-FA (200 μg/mL) for 6 h. Subsequently, the medium was removed and washed with PBS twice, and then the cells were fixed with paraformaldehyde solution (4%) for 15 min. The cytoskeletons were stained with fluorescein isothiocyanate (FITC)-phalloidin for 20 min, and the

nuclei were stained with DAPI for 10 min. The cells were observed under an FV-1000 confocal microscope (Olympus, Tokyo, Japan).

Additionally, the uptake of PSB@NP-FA by RAW 264.7 and Colon-26 cells was detected using flow cytometry quantitatively. After cell adhesion, NPs were co-incubated with cells for 6 h, the medium was removed, and the cells were collected. The fluorescence intensity of cells labeled by DiL was quantified by flow cytometry (Beckman Coulter, CA, USA), which reflected the uptake efficiency of PSB@NP-FA by RAW 264.7 and Colon-26 cells.

In vivo biodistribution study of PSB@NP-FA

To study the biodistribution of PSB@NP-FA *in vivo*, DiR-labeled PSB@NP-FA were administered intravenously to healthy control mice and DSS-induced colitis mice. Biodistribution of DiR-labeled PSB@NP or PSB@NP-FA in mice was acquired at each time point using the Living Image software (PerkinElmer, Waltham, MA, USA). Finally, mice were sacrificed, and the main organs (liver, heart, lung, spleen, kidney, and colon) were obtained and imaged. The corresponding intensities were quantitatively assessed and displayed by histogram.

In vitro cytotoxicity evaluation of NP

The cytotoxicity of Blank@NP and PSB@NP-FA was assessed by the MTT assay. Briefly, RAW 264.7 cells were cultured in a 96-well plate at the concentration of 5×10^4 cells/mL (100 μL/well). After incubating overnight, NP with varying concentrations was added. At 24 or 48 h later, 20 μL of MTT (5 mg/mL) was added to each well and incubated for a further 4 h. Finally, the medium was removed, and DMSO (150 μL/well) was added to dissolve formazan. The absorbance was measured at 490 nm using an enzyme-linked immunoassay analyzer (BioTek Synergy, USA).

In vivo biocompatibility evaluation of Blank@NP

To evaluate the biocompatibility of Blank@NP *in vivo*, mice were administrated with Blank@NP intravenously for seven consecutive days. The body weight of the mice was recorded daily. At the end of the experiment, the mice were sacrificed, and the main organs (heart, kidney, liver, lung, and spleen) and colons were dissected and fixed with formalin. After formalin fixation for more than 1 day, tissues were dehydrated and paraffin-embedded. H&E staining was used for histological evaluations.

The whole blood and serum of the mice were collected for typical routine blood tests and biochemistry analyses. The routine blood tests include red blood cells, white blood cells, platelets, and hemoglobin count. The biochemistry analyses include alanine aminotransferase, aspartate aminotransferase, serum creatinine, and blood urea nitrogen.

Colitis model of mice

C57BL/6 mice (6–8 weeks) provided by the Medical Experimental Animal Center of Xi'an Jiaotong University (Shaanxi Province, China) were used to build the colitis mice model. Colitis was induced by adding 2.5% (w/v) DSS to drinking water for 7 days. To evaluate the therapeutic efficacy of PSB@NP-FA and DEX/PSB@NP-FA, mice with DSS treatment received intravenous injections every other day. Injection doses of PSB@NP-FA ranged from 10 to 30 mg/kg. The dose of DEX was 5 mg/kg, often used as the optimal dose in mouse inflammatory models. DAI includes body weight loss, rectal bleeding, and stool consistency and can be used as an indicator of disease activity. By recording three indexes in DAI of mice during the experiment every day, the combined scoring statistics can reflect the situation of the UC model and the treatment effect of NP. At the end of the experiment, the mice were sacrificed to obtain blood samples, main organs, and colons. The length of colons in each group was measured and photographed. The tissue samples were stored in formalin for further tissue sections or stored at −80°C for further qPCR and MPO analysis. All experiments complied with the institutional Animal Care and Use Committee at Xi'an Jiaotong University.

Isolation of LPLs

To isolate LPLs, the feces in the colon were first removed by flushing with DMEM and 10% fetal bovine serum (FBS)s. Then the colon was longitudinally dissected and cut into pieces (∼0.5 cm). Solution I (4 mL) was added to the colon pieces and shaken at 220 rpm for 30 min at 37°C. The samples were then vortexed for 10 s and passed through a gray mesh (100 μm). Colon pieces on the gray mesh were returned to the original tube, and the supernatant was collected in a new tube. These steps (incubation, vortex, and grinding) were repeated more than once. Solution II was added to the colon pieces and incubated at 37°C for 45 min under shaking (220 rpm). Finally, the colon pieces were passed through the gray mesh and centrifuged at 1,500 rpm for 5 min at 4°C. The fraction contained the LPLs and was stained by desired markers for flow cytometry analysis. Solutions I and II were as follow:

Solution I: DMEM + 5% FBS + 5 mM EDTA + 0.15 mg/mL (1 mM) DTT.

Solution II: 1640 + 10% FBS + 120 U/mL collagenase IV + 0.5 mg/mL DNase I

Antibodies

APC/Cy7 anti-mouse CD4, FITC anti-mouse CD8, PE/Cy5 anti-mouse TCRβ (T cell receptor beta), PE/Cy7 anti-mouse CD44, APC anti-mouse CD62L, PE anti-mouse CD25, FITC anti-mouse CD11b, PE/Cy5 anti-mouse GR1, APC anti-mouse CD206, PE anti-mouse iNOS, APC/Cy7 anti-mouse F4/80, PE/Cy7 anti-mouse IFN-γ, PB anti-mouse IL-17, APC anti-mouse TNF-α, FITC anti-mouse CD11c, PE/Cy7 anti-mouse MHC-II, APC anti-mouse CD80, and APC/Cy7 anti-mouse B220. All reagents were purchased from BioLegend.

Flow cytometry

Cells taken from the mice were made into a cell suspension. For cell surface analysis, a total of $1 \sim 5 \times 10^6$ cells were stained with

indicated antibodies in the dark at 4°C for 30 min. After washing with cold fluorescence-activated cell sorting (FACS) buffer (1× PBS supplemented with 2% FBS), cells were analyzed using CytoFLEX flow cytometer (Beckman Coulter), and the data were analyzed using FlowJo software (CytExpert).

Statistical analysis

The data are presented as the mean SDs in triplicate. The student's t test was used to analyze the difference between the two groups. Statistical analysis was performed using GraphPad Prism 7 software and were defined as *p < 0.05, **p < 0.01, and ***p < 0.001.

DATA AND CODE AVAILABILITY

Data is available online or from the author.

SUPPLEMENTAL INFORMATION

Supplemental information can be found online at https://doi.org/10.1016/j.ymthe.2023.02.017.

ACKNOWLEDGMENTS

This work was supported by the National Natural Science Foundation of China (no. 82000523), the Scientific Research Fund of National Health Commission-Major Health Science and Technology Program of Zhejiang Province (WKJ-ZJ-2205), the Zhejiang Provincial Natural Science Foundation of China (LR22H160008), and the Young Talent Support Plan of Xi'an Jiaotong University, China (no. YX6J001). We also thank Dr. Zijun Ren at the Instrument Analysis Center of Xi'an Jiaotong University for assisting with TEM analysis and Dr. Xiaofei Wang at the experimental biomedical center of Xi'an Jiaotong University for his kind assistance with the instrument operation and data analysis.

AUTHOR CONTRIBUTIONS

Z.M.Z. and Y.X.J. contributed to design and completion of the study. Z.X.Z., D.Z.C., G.B.W., and Y.M. made contributions in cell experiments and animal experiments. M.Y.N. and Z.Y.Y. participated in grammar revision. Z.Y.J. guided the data analysis. M.L.Z., X.Q.R., and T.K.S. supported this study.

DECLARATION OF INTERESTS

The authors declare no competing interests.

REFERENCES

1. Shi, H., Zhao, X., Gao, J., Liu, Z., Liu, Z., Wang, K., and Jiang, J. (2020). Acid-resistant ROS-responsive hyperbranched polythioether micelles for ulcerative colitis therapy. Chin. Chem. Lett. *31*, 3102–3106.

2. Wang, X., Gu, H., Zhang, H., Xian, J., Li, J., Fu, C., Zhang, C., and Zhang, J. (2021). Oral core-shell nanoparticles embedded in hydrogel microspheres for the efficient site-specific delivery of magnolol and enhanced antiulcerative colitis therapy. ACS Appl. Mater. Inter. *13*, 33948–33961.

3. Ansari, M.M., Ahmad, A., Kumar, A., Alam, P., Khan, T.H., Jayamurugan, G., Raza, S.S., and Khan, R. (2021). Aminocellulose-grafted-polycaprolactone coated gelatin nanoparticles alleviate inflammation in rheumatoid arthritis: a combinational therapeutic approach. Carbohydr. Polym. *258*, 117600.

4. Xu, Y., Zhu, B.W., Li, X., Li, Y.F., Ye, X.M., and Hu, J.N. (2022). Glycogen-based pH and redox sensitive nanoparticles with ginsenoside Rh2 for effective treatment of ulcerative colitis. Biomaterials *280*, 121077.

5. Chen, Q., Luo, R., Han, X., Zhang, J., He, Y., Qi, S., Pu, X., Nie, W., Dong, L., Xu, H., et al. (2021). Entrapment of macrophage-target nanoparticles by yeast microparticles for rhein delivery in ulcerative colitis treatment. Biomacromolecules *22*, 2754–2767.

6. Li, C., Zhao, Y., Cheng, J., Guo, J., Zhang, Q., Zhang, X., Ren, J., Wang, F., Huang, J., Hu, H., et al. (2019). A proresolving peptide nanotherapy for site-specific treatment of inflammatory bowel disease by regulating proinflammatory microenvironment and gut microbiota. Adv. Sci. *6*, 1900610.

7. Wang, Y., Li, L., Zhao, W., Dou, Y., An, H., Tao, H., Xu, X., Jia, Y., Lu, S., Zhang, J., and Hu, H. (2018). Targeted therapy of atherosclerosis by a broad-spectrum reactive oxygen species scavenging nanoparticle with intrinsic anti-inflammatory activity. ACS Nano *12*, 8943–8960.

8. Huang, Y., Canup, B.S.B., Gou, S., Chen, N., Dai, F., Xiao, B., and Li, C. (2021). Oral nanotherapeutics with enhanced mucus penetration and ROS-responsive drug release capacities for delivery of curcumin to colitis tissues. J. Mater. Chem. B *9*, 1604–1615.

9. Ahn, J.Y., Lee, K.H., Choi, C.H., Kim, J.W., Lee, H.W., Kim, J.W., Kim, M.K., Kwon, G.Y., Han, S., Kim, S.E., et al. (2014). Colonic mucosal immune activity in irritable bowel syndrome: comparison with healthy controls and patients with ulcerative colitis. Dig. Dis. Sci. *59*, 1001–1011.

10. Roda, G., Dahan, S., Mezzanotte, L., Caponi, A., Roth-Walter, F., Pinn, D., and Mayer, L. (2009). Defect in CEACAM family member expression in Crohn's disease IECs is regulated by the transcription factor SOX9. Inflamm. Bowel Dis. *15*, 1775–1783.

11. Doering, J., Begue, B., Lentze, M.J., Rieux-Laucat, F., Goulet, O., Schmitz, J., Cerf-Bensussan, N., and Ruemmele, F.M. (2004). Induction of T lymphocyte apoptosis by sulphasalazine in patients with Crohn's disease. Gut *53*, 1632–1638.

12. Lord, J.D., Shows, D.M., Chen, J., and Thirlby, R.C. (2015). Human blood and mucosal regulatory T cells express activation markers and inhibitory receptors in inflammatory bowel disease. PLoS One *10*, e0136485.

13. Yashiro, T., Yura, S., Tobita, A., Toyoda, Y., Kasakura, K., and Nishiyama, C. (2020). Pterostilbene reduces colonic inflammation by suppressing dendritic cell activation and promoting regulatory T cell development. FASEB J. *34*, 14810–14819.

14. Li, X., Lu, C., Yang, Y., Yu, C., and Rao, Y. (2020). Site-specific targeted drug delivery systems for the treatment of inflammatory bowel disease. Biomed. Pharmacother. *129*, 110486.

15. Rogler, G. (2017). Resolution of inflammation in inflammatory bowel disease. Lancet Gastroenterol. Hepatol. *2*, 521–530.

16. Lin, H.S., Yue, B.D., and Ho, P.C. (2009). Determination of pterostilbene in rat plasma by a simple HPLC-UV method and its application in pre-clinical pharmacokinetic study. Biomed. Chromatogr. *23*, 1308–1315.

17. Chan, C.N., Trinité, B., and Levy, D.N. (2017). Potent inhibition of HIV-1 replication in resting CD4 T cells by resveratrol and pterostilbene. Antimicrob. Agents Chemother. *61*, e00408–e00417.

18. Nikhil, K., Sharan, S., Palla, S.R., Sondhi, S.M., Peddinti, R.K., and Roy, P. (2015). Understanding the mode of action of a pterostilbene derivative as anti-inflammatory agent. Int. Immunopharmacol. *28*, 10–21.

19. Paul, S., Rimando, A.M., Lee, H.J., Ji, Y., Reddy, B.S., and Suh, N. (2009). Anti-inflammatory action of pterostilbene is mediated through the p38 mitogen-activated protein kinase pathway in colon cancer cells. Cancer Prev. Res. *2*, 650–657.

20. Zou, Y., Wang, X., Bi, D., Fu, J., Han, J., Guo, Y., Feng, L., and Han, M. (2021). Pterostilbene nanoparticles with small particle size show excellent anti-breast cancer activity *in vitro* and *in vivo*. Nanotechnology *32*, 325102.

21. Remsberg, C.M., Yáñez, J.A., Ohgami, Y., Vega-Villa, K.R., Rimando, A.M., and Davies, N.M. (2008). Pharmacometrics of pterostilbene: preclinical pharmacokinetics and metabolism, anticancer, antiinflammatory, antioxidant and analgesic activity. Phytother. Res. *22*, 169–179.

22. McCormack, D., and McFadden, D. (2013). A review of pterostilbene antioxidant activity and disease modification. Oxid. Med. Cell. Longev. *2013*, 575482.

23. Wang, J., Zhao, H., Lv, K., Zhao, W., Zhang, N., Yang, F., Wen, X., Jiang, X., Tian, J., Liu, X., et al. (2021). Pterostilbene ameliorates DSS-induced intestinal epithelial

barrier loss in mice via suppression of the NF-kappaB-Mediated MLCK-MLC signaling pathway. J. Agric. Food Chem. *69*, 3871–3878.

24. Bethune, S.J., Schultheiss, N., and Henck, J.-O. (2011). Improving the poor aqueous solubility of nutraceutical compound pterostilbene through cocrystal formation. Cryst. Growth Des. *11*, 2817–2823.
25. Gao, C., Yu, S., Zhang, X., Dang, Y., Han, D.D., Liu, X., Han, J., and Hui, M. (2021). Dual functional eudragit((R)) S100/L30D-55 and PLGA colon-targeted nanoparticles of iridoid glycoside for improved treatment of induced ulcerative colitis. Int. J. Nanomedicine *16*, 1405–1422.
26. Naeem, M., Choi, M., Cao, J., Lee, Y., Ikram, M., Yoon, S., Lee, J., Moon, H.R., Kim, M.S., Jung, Y., and Yoo, J.W. (2015). Colon-targeted delivery of budesonide using dual pH- and time-dependent polymeric nanoparticles for colitis therapy. Drug Des. Devel. Ther. *9*, 3789–3799.
27. Wu, P., Zhou, Q., Zhu, H., Zhuang, Y., and Bao, J. (2020). Enhanced antitumor efficacy in colon cancer using EGF functionalized PLGA nanoparticles loaded with 5-Fluorouracil and perfluorocarbon. BMC Cancer *20*, 354.
28. Ling, G., Zhang, P., Zhang, W., Sun, J., Meng, X., Qin, Y., Deng, Y., and He, Z. (2010). Development of novel self-assembled DS-PLGA hybrid nanoparticles for improving oral bioavailability of vincristine sulfate by P-gp inhibition. J. Control Release *148*, 241–248.
29. Zheng, Y., You, X., Guan, S., Huang, J., Wang, L., Zhang, J., and Wu, J. (2019). Poly(Ferulic acid) with an anticancer effect as a drug nanocarrier for enhanced colon cancer therapy. Adv. Funct. Mater. *29*, 1808646.
30. Gou, S., Huang, Y., Wan, Y., Ma, Y., Zhou, X., Tong, X., Huang, J., Kang, Y., Pan, G., Dai, F., and Xiao, B. (2019). Multi-bioresponsive silk fibroin-based nanoparticles with on-demand cytoplasmic drug release capacity for CD44-targeted alleviation of ulcerative colitis. Biomaterials *212*, 39–54.
31. Arruda, D.C., Lachagès, A.M., Demory, H., Escriou, G., Lai-Kuen, R., Dugas, P.Y., Hoffmann, C., Bessoles, S., Sarrabayrouse, G., Malachias, A., et al. (2022). Spheroplexes: hybrid PLGA-cationic lipid nanoparticles, for in vitro and oral delivery of siRNA. J. Control Release *350*, 228–243.
32. Ali, H., Weigmann, B., Neurath, M.F., Collnot, E.M., Windbergs, M., and Lehr, C.M. (2014). Budesonide loaded nanoparticles with pH-sensitive coating for improved mucosal targeting in mouse models of inflammatory bowel diseases. J. Control Release *183*, 167–177.
33. Shrestha, N., Xu, Y., Prévost, J.R.C., McCartney, F., Brayden, D., Frédérick, R., Beloqui, A., and Préat, V. (2022). Impact of PEGylation on an antibody-loaded nanoparticle-based drug delivery system for the treatment of inflammatory bowel disease. Acta Biomater. *140*, 561–572.
34. Zhang, M., Xu, C., Liu, D., Han, M.K., Wang, L., and Merlin, D. (2018). Oral delivery of nanoparticles loaded with ginger active compound, 6-shogaol, attenuates ulcerative colitis and promotes wound healing in a murine model of ulcerative colitis. J. Crohn's. Colitis *12*, 217–229.
35. Zhang, K., Yang, P.P., Zhang, J.P., Wang, L., and Wang, H. (2017). Recent advances of transformable nanoparticles for theranostics. Chin. Chem. Lett. *28*, 1808–1816.
36. Yi, Y.S. (2016). Folate receptor-targeted diagnostics and therapeutics for inflammatory diseases. Immune Netw. *16*, 337–343.
37. Ledermann, J.A., Canevari, S., and Thigpen, T. (2015). Targeting the folate receptor: diagnostic and therapeutic approaches to personalize cancer treatments. Ann. Oncol. *26*, 2034–2043.
38. Chung, C.H., Jung, W., Keum, H., Kim, T.W., and Jon, S. (2020). Nanoparticles derived from the natural antioxidant rosmarinic acid ameliorate acute inflammatory bowel disease. ACS Nano *14*, 6887–6896.
39. He, G., Yan, X., Miao, Z., Qian, H., Ma, Y., Xu, Y., Gao, L., Lu, Y., and Zha, Z. (2020). Anti-inflammatory catecholic chitosan hydrogel for rapid surgical trauma healing and subsequent prevention of tumor recurrence. Chin. Chem. Lett. *31*, 1807–1811.
40. Zhang, M., Viennois, E., Prasad, M., Zhang, Y., Wang, L., Zhang, Z., Han, M.K., Xiao, B., Xu, C., Srinivasan, S., and Merlin, D. (2016). Edible ginger-derived nanoparticles: a novel therapeutic approach for the prevention and treatment of inflammatory bowel disease and colitis-associated cancer. Biomaterials *101*, 321–340.
41. Coombes, J.L., and Powrie, F. (2008). Dendritic cells in intestinal immune regulation. Nat. Rev. Immunol. *8*, 435–446.
42. Clough, J.N., Omer, O.S., Tasker, S., Lord, G.M., and Irving, P.M. (2020). Regulatory T-cell therapy in Crohn's disease: challenges and advances. Gut *69*, 942–952.
43. Kapetanovic, I.M., Muzzio, M., Huang, Z., Thompson, T.N., and McCormick, D.L. (2011). Pharmacokinetics, oral bioavailability, and metabolic profile of resveratrol and its dimethylether analog, pterostilbene, in rats. Cancer Chemother. Pharmacol. *68*, 593–601.
44. Nunes, S., Danesi, F., Del Rio, D., and Silva, P. (2018). Resveratrol and inflammatory bowel disease: the evidence so far. Nutr. Res. Rev. *31*, 85–97.
45. Kim, H., Seo, K.H., and Yokoyama, W. (2020). Chemistry of pterostilbene and its metabolic effects. J. Agric. Food Chem. *68*, 12836–12841.
46. Hou, Y., Xie, G., Miao, F., Ding, L., Mou, Y., Wang, L., Su, G., Chen, G., Yang, J., and Wu, C. (2014). Pterostilbene attenuates lipopolysaccharide-induced learning and memory impairment possibly via inhibiting microglia activation and protecting neuronal injury in mice. Prog. Neuropsychopharmacol. Biol. Psychiatry *54*, 92–102.
47. Koh, Y.C., Lee, P.S., Kuo, Y.L., Nagabhushanam, K., Ho, C.T., and Pan, M.H. (2021). Dietary pterostilbene and resveratrol modulate the gut microbiota influenced by circadian rhythm dysregulation. Mol. Nutr. Food Res. *65*, 2100434.
48. Chen, Y., Zhang, H., Chen, Y., Jia, P., Ji, S., Zhang, Y., and Wang, T. (2021). Resveratrol and its derivative pterostilbene ameliorate intestine injury in intrauterine growth-retarded weanling piglets by modulating redox status and gut microbiota. J. Anim. Sci. Biotechnol. *12*, 70–1542.
49. Lee, Y., Sugihara, K., Gillilland, M.G., Jon, S., Kamada, N., and Moon, J.J. (2020). Hyaluronic acid-bilirubin nanomedicine for targeted modulation of dysregulated intestinal barrier, microbiome and immune responses in colitis. Nat. Mater. *19*, 118–126.
50. Yang, M., Zhang, F., Yang, C., Wang, L., Sung, J., Garg, P., Zhang, M., and Merlin, D. (2020). Oral targeted delivery by nanoparticles enhances efficacy of an Hsp90 inhibitor by reducing systemic exposure in murine models of colitis and colitis-associated cancer. J. Crohns Colitis *14*, 130–141.
51. Yang, B., Chen, Y., and Shi, J. (2019). Reactive oxygen species (ROS)-Based nanomedicine. Chem. Rev. *119*, 4881–4985.
52. Zhao, Y., Xie, R., Yodsanit, N., Ye, M., Wang, Y., Wang, B., Guo, L.W., Kent, K.C., and Gong, S. (2021). Hydrogen peroxide-responsive platelet membrane-coated nanoparticles for thrombus therapy. Biomater. Sci. *9*, 2696–2708.
53. Shalon, L., Gulwani-Akolkar, B., Fisher, S.E., Akolkar, P.N., Panja, A., Mayer, L., and Silver, J. (1994). Evidence for an altered T-cell receptor repertoire in Crohn's disease. Autoimmunity *17*, 301–307.
54. Ding, X., Bin, P., Wu, W., Chang, Y., and Zhu, G. (2020). Tryptophan metabolism, regulatory T cells, and inflammatory bowel disease: a mini review. Mediators Inflamm. *2020*, 9706140.
55. Shin, B., Kress, R.L., Kramer, P.A., Darley-Usmar, V.M., Bellis, S.L., and Harrington, L.E. (2018). Effector CD4 T cells with progenitor potential mediate chronic intestinal inflammation. J. Exp. Med. *215*, 1803–1812.
56. Boden, E.K., and Lord, J.D. (2017). CD4 T cells in IBD: crossing the line? Dig. Dis. Sci. *62*, 2208–2210.
57. Tindemans, I., Joosse, M.E., and Samsom, J.N. (2020). Dissecting the heterogeneity in T-cell mediated inflammation in IBD. Cells *9*, 110.
58. Brasseit, J., Althaus-Steiner, E., Faderl, M., Dickgreber, N., Saurer, L., Genitsch, V., Dolowschiak, T., Li, H., Finke, D., Hardt, W.D., et al. (2016). CD4 T cells are required for both development and maintenance of disease in a new mouse model of reversible colitis. Mucosal Immunol. *9*, 689–701.
59. Yu, X., Zhang, H., Yu, L., Liu, M., Zuo, Z., Han, Q., Zhang, J., Tian, Z., and Zhang, C. (2018). Intestinal lamina propria CD4(+) T cells promote bactericidal activity of macrophages via galectin-9 and tim-3 interaction during Salmonella enterica serovar typhimurium infection. Infect. Immun. *86*, e817.

YMTHE, Volume *31*

Supplemental Information

Reactive oxygen species-responsive nanocarrier ameliorates murine colitis by intervening colonic innate and adaptive immune responses

Xiangji Yan, Lingzhang Meng, Xingzhe Zhang, Zhichao Deng, Bowen Gao, Yujie Zhang, Mei Yang, Yana Ma, Yuanyuan Zhang, Kangsheng Tu, Mingzhen Zhang, and Qiuran Xu

Supplemental data

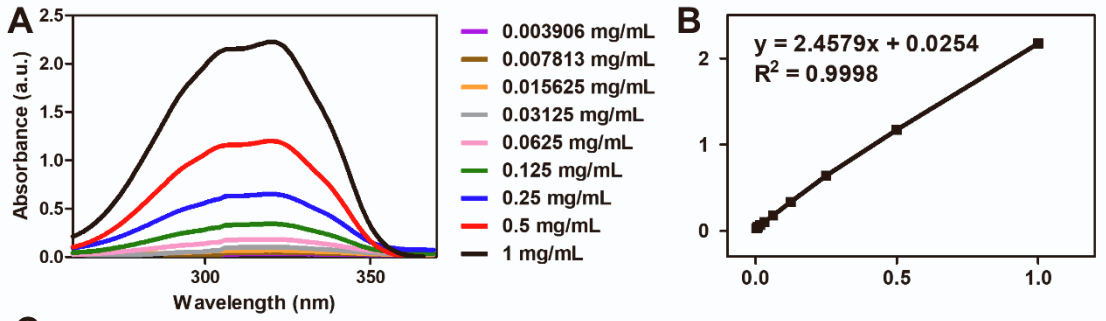

C

	Entrapment efficiency (EE%)	Loading capacity (LC%)
PSB@NP (2.5mg)	85.27%	3.74%
PSB@NP (5mg)	50.18%	3.38%
PSB@NP (7.5mg)	48.44%	3.02%
PSB@NP (10mg)	18.89%	1.36%

Figure S1. The entrapment efficiency and loading capacity of PSB in PSB@NPs were measured by a UV-vis spectrophotometer. (A) Absorption peaks of PSB with different concentrations. (B) The standard curve. (C) The entrapment efficiency and loading capacity of different dosages of PSB in PSB@NP.

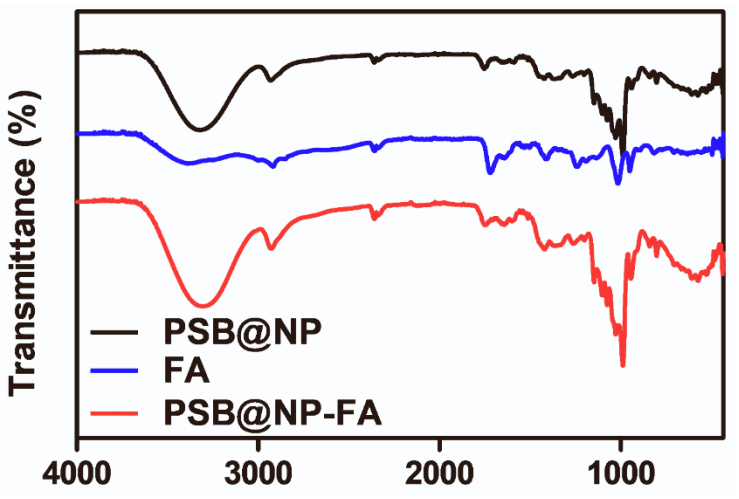

Figure S2. FTIR spectra of PSB@NP, FA and PSB@NP-FA.

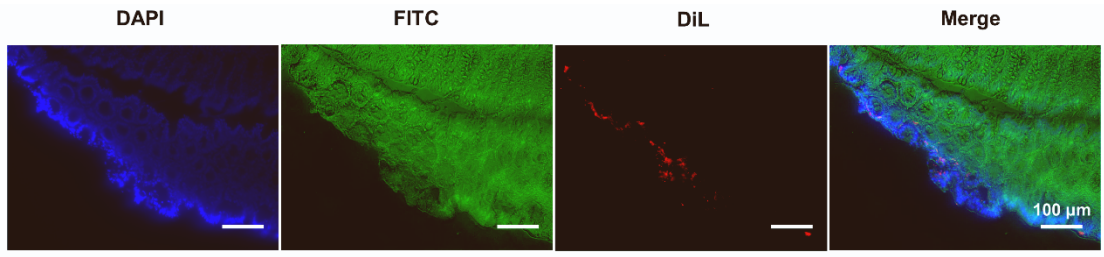

Figure S3. Frozen sections of colon tissues uptake with DiL labeled-NP. Phalloidin-FITC (green) represents actin and DAPI (blue) for nuclei. Scale bar: 100 μm.

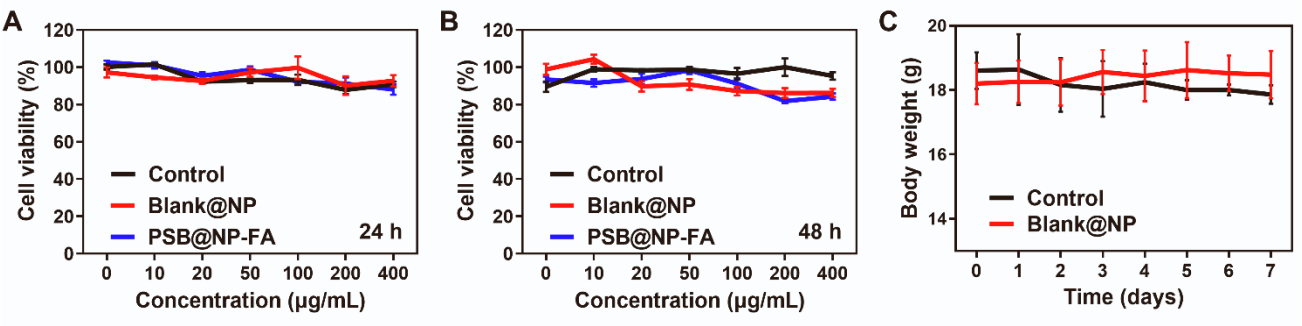

Figure S4. Biocompatibility of NP was assessed *in vitro* and *in vivo*. (A) *In vitro* cytotoxicity of different concentrations of Blank@NP and PSB@NP-FA in RAW 264.7 cells after incubating for 24 h and 48 h, as determined by MTT assay. (B) *In vitro* cytotoxicity of different concentrations of Blank@NP and PSB@NP-FA in RAW 264.7 cells after incubating for 48 h. (C) Daily changes in body weight of healthy mice treated daily for 7 days with Blank@NP or saline (n = 5).

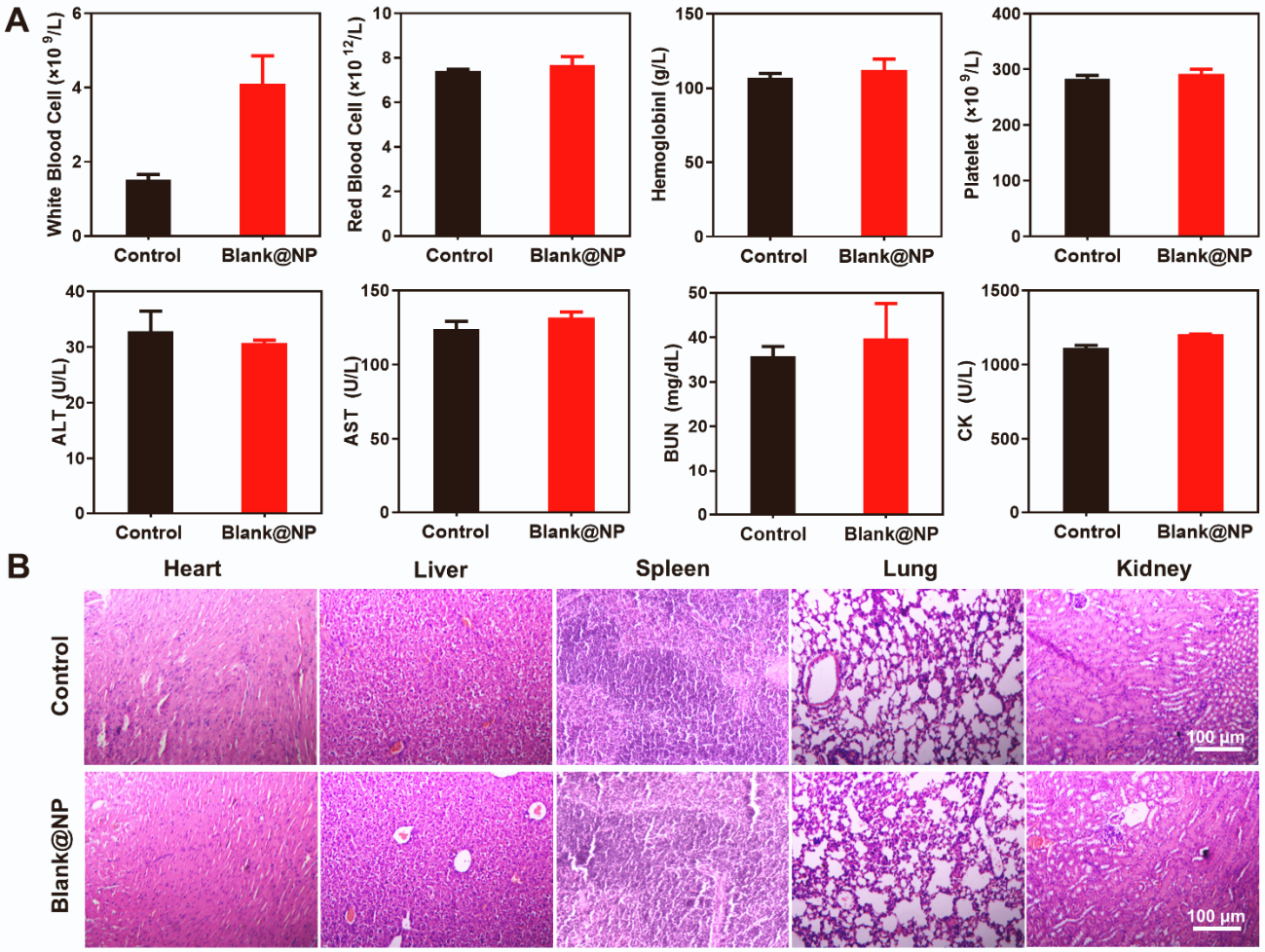

Figure S5. Biocompatibility evaluation of NP. (A) Biocompatibility evaluation was evaluated by analyzing hematology and biochemistry parameters, (n = 5). (B) Representative photomicrographs of H&E-stained sections of the major organs (heart, kidney, liver, lung, and spleen). Scale bar: 100 μm.

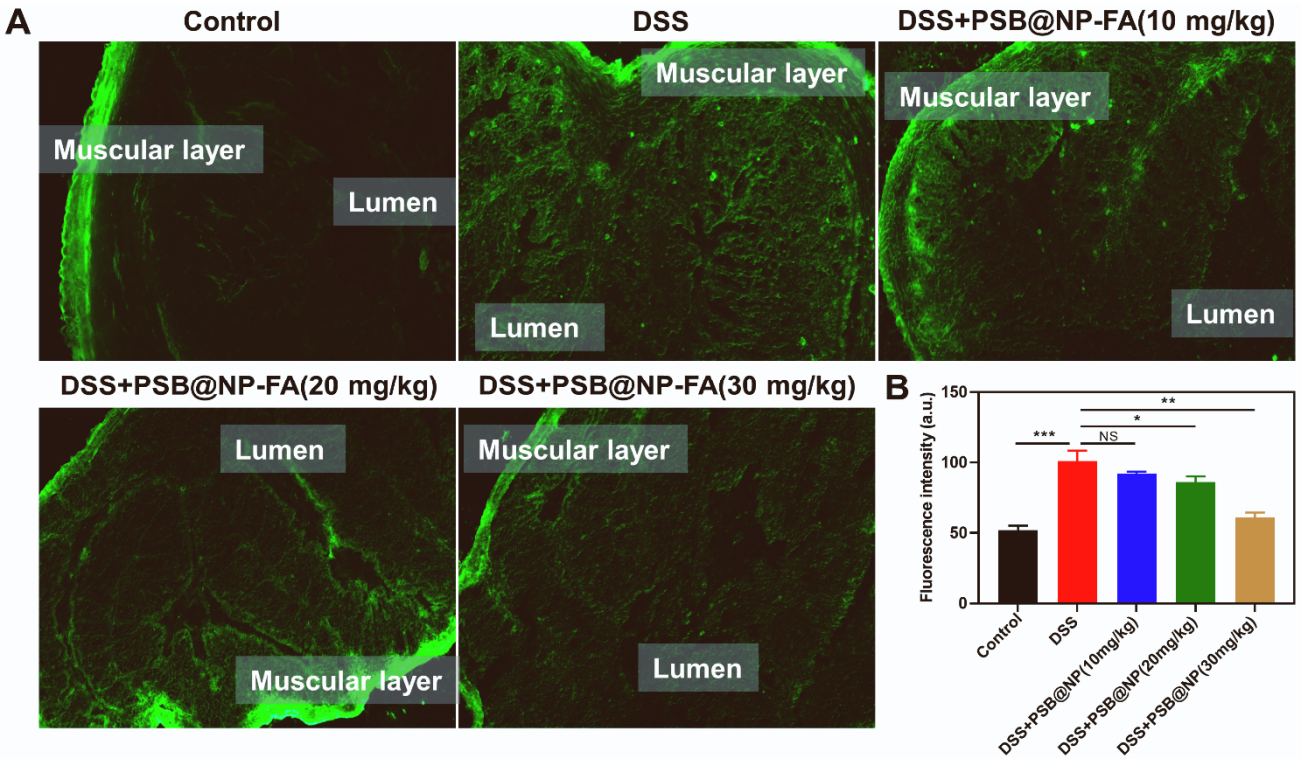

Figure S6. The level of ROS *in vivo* was detected by ROS probe DCFH-DA. (A) Fluorescence intensity of frozen sections of colon tissues in different treatment groups. (B) Histogram of fluorescence signal statistics of different groups.

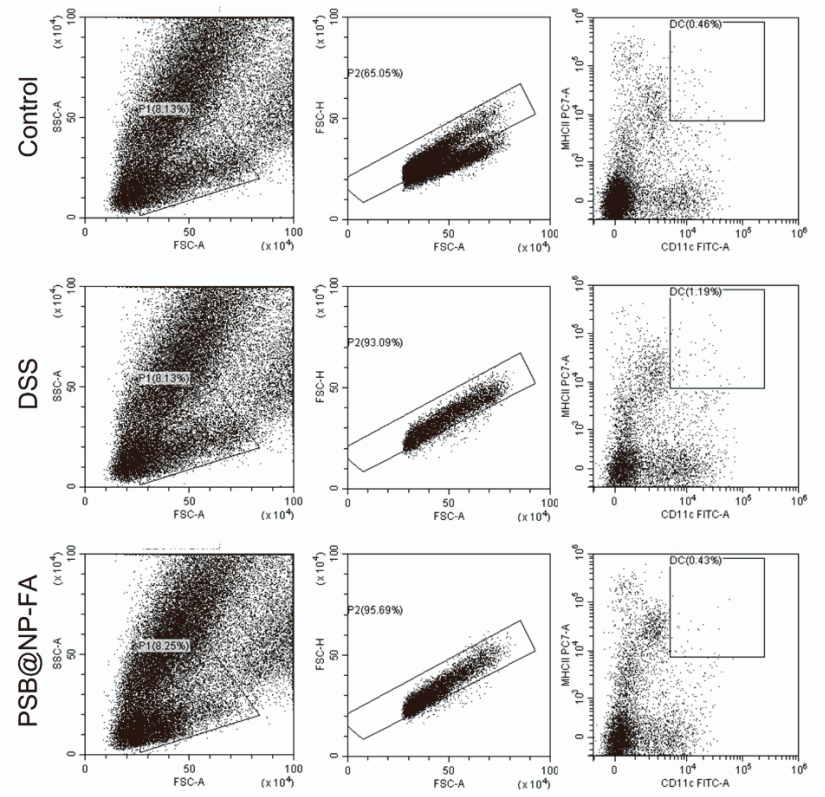

Figure S7. Scatter plots of Figure 5A.

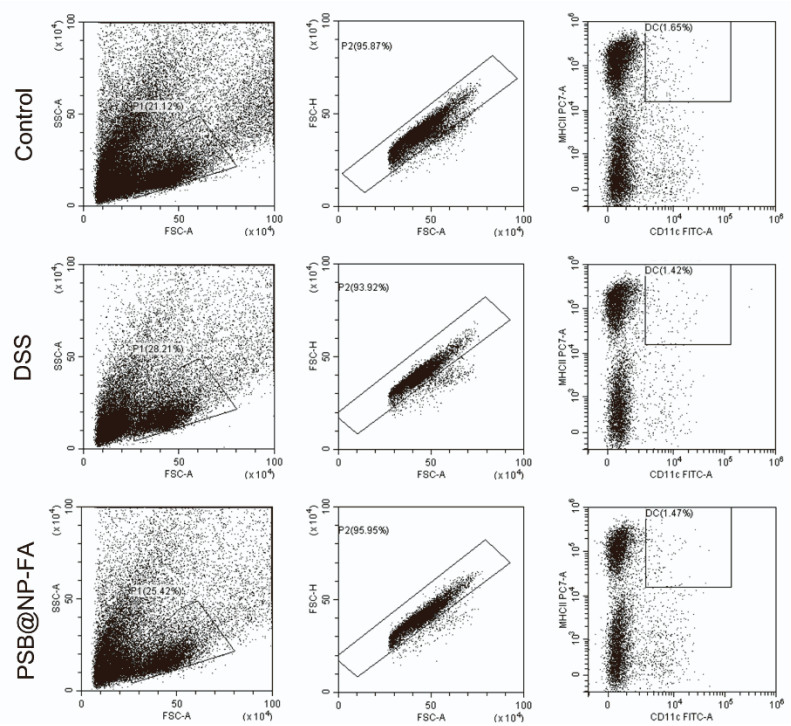

Figure S8. Scatter plots of Figure 5B.

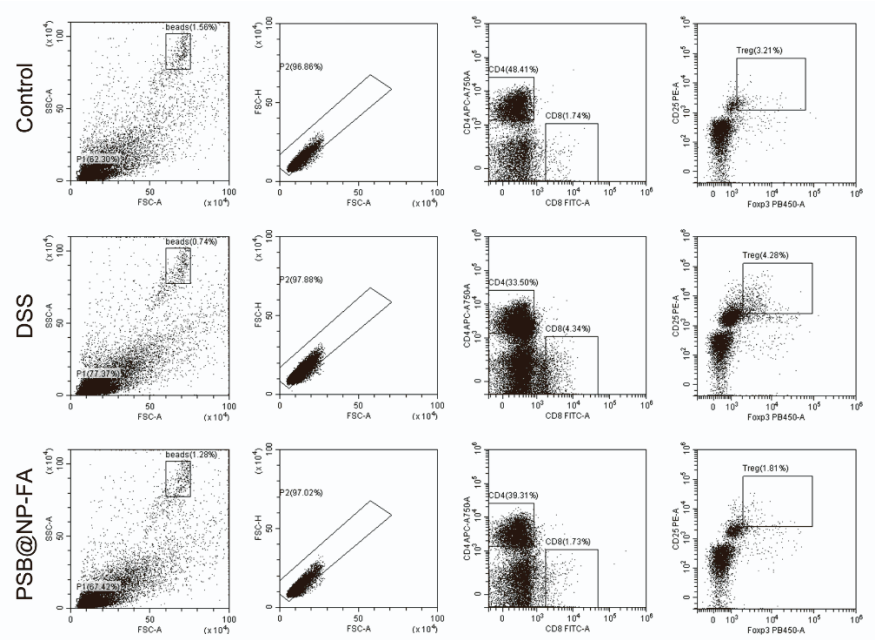

Figure S9. Scatter plots of Figure 6C.

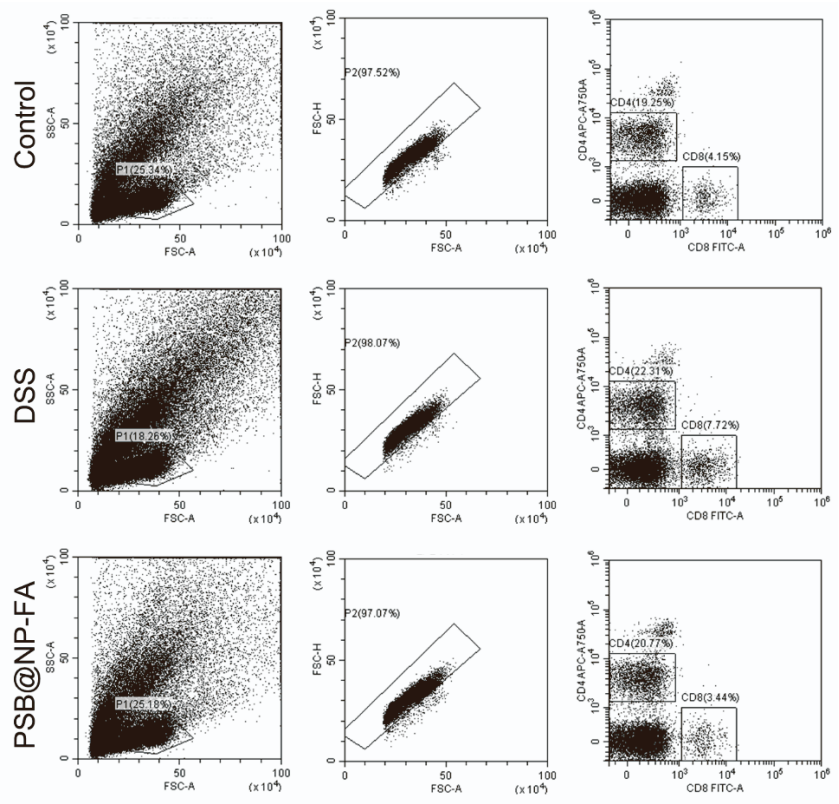

Figure S10. Scatter plots of Figure 6E.

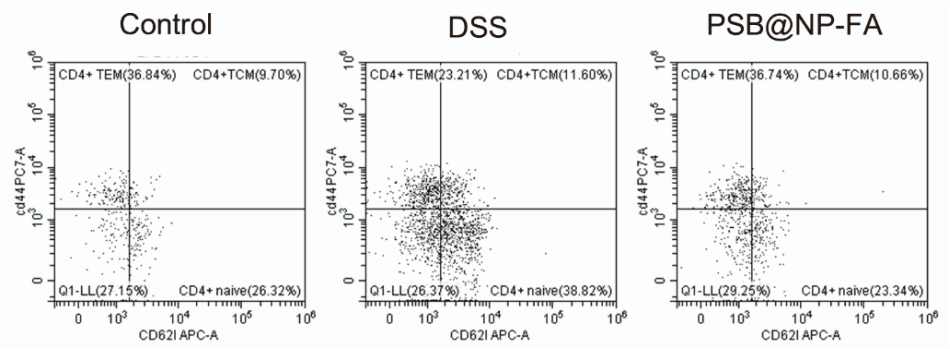

Figure S11. Scatter plots of Figure 6 FGH.

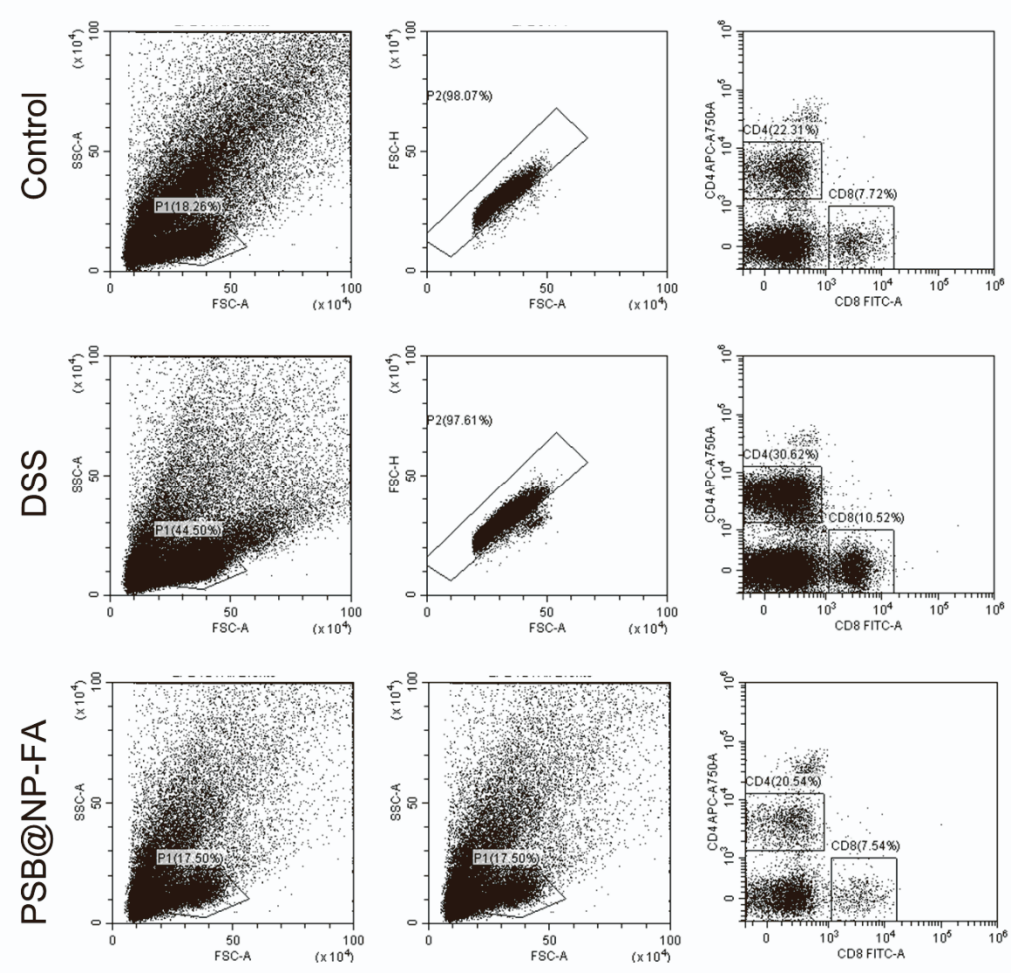

Figure S12. Scatter plots of Figure 6M.

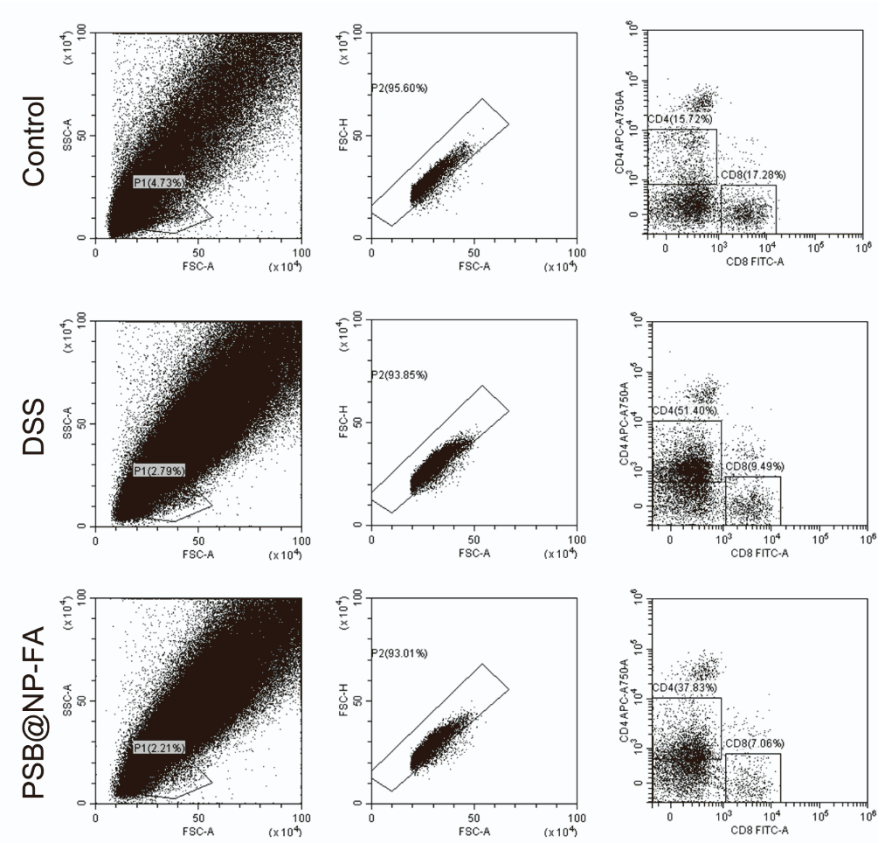

Figure S13. Scatter plots of Figure 6O.

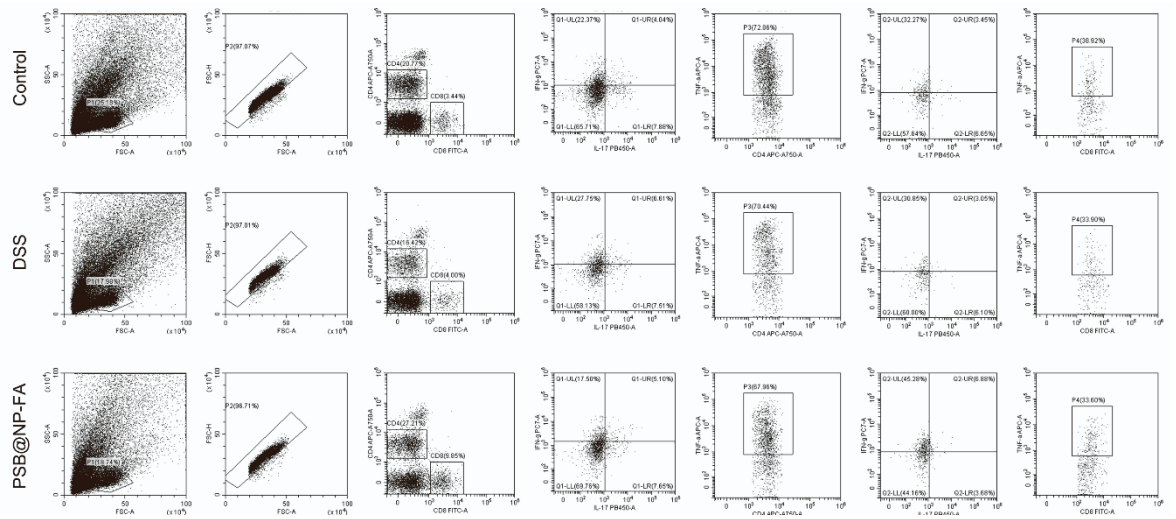

Figure S14. Scatter plots of Figure 7.

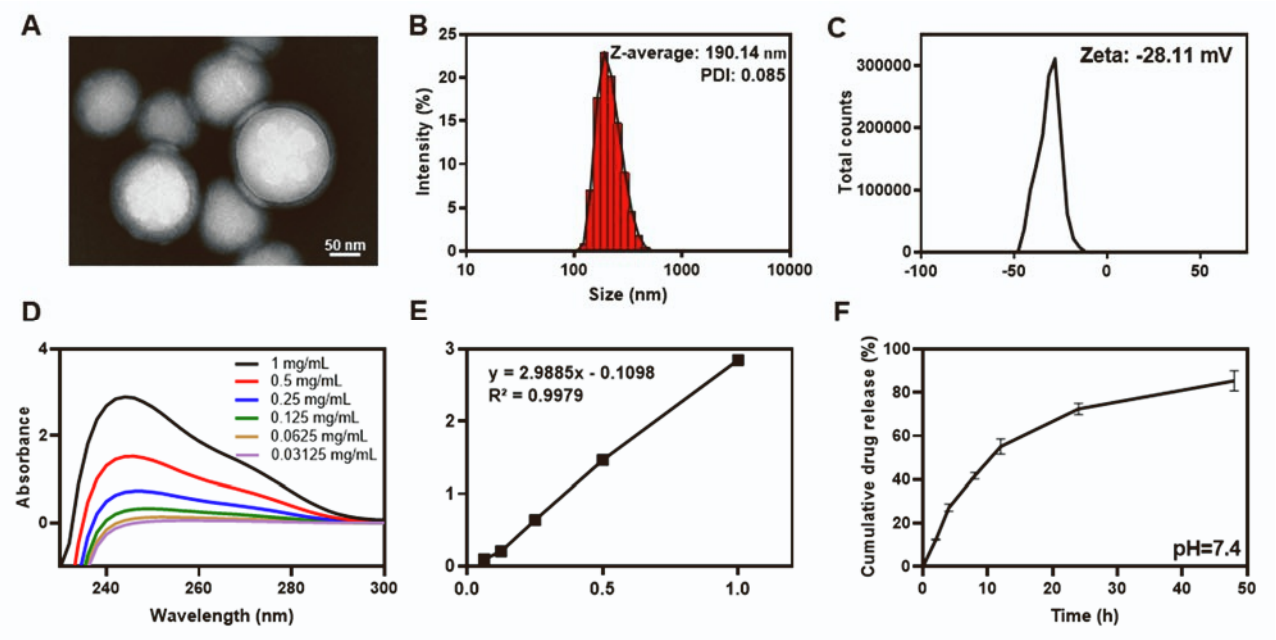

Figure S15. Characterization and *in vitro* drug-release profiles of DEX/PSB@NP-FA. (A) Representative TEM images of DEX/PSB@NP-FA. Scale bar: 50 nm. (B) Representative size distribution and PDI of DEX/PSB@NP-FA, (n=3). (C) Zeta potential of DEX/PSB@NP-FA, (n=3). (D) UV-vis absorption spectra of DEX with different concentrations. (E) The standard curve of DEX. (F) The release profile of DEX from PLGA (pH 7.4), (n=3).

Table S1. Primers used for Real-time PCR.

Gene	Forward primer (5'-3')	Reverse primer(5'-3')
TNF-α	AGGCTGCCCCGACTACGT	GACTTTCTCCTGGTATGAGATAGCAAA
IL-6	ACAAGTCGGAGGCTTAATTACACAT	TTGCCATTGCACAACTCTTTTC
IL-1β	TCGCTCAGGGTCACAAGAAA	CATCAGAGGCAAGGAGGA AAAC
IL-12	GCCAGTACACCTGCCACAAA	TGTGGAGCAGCAGATGTGAGT
IL-10	GGTTGCCAAGCCTTATCGGA	CTTCTCACCCAGGGAATTCA
36b4	TCCAGGCTTTGGGCATCA	CTTTATCAGCTGCACATCACTCAGA